# STUDY OF SCHOTTKY AND POOLE-FRENKEL CONDUCTION MECHANISM IN FE3O4-GAMMA-FE2O3/SIO2/N-TYPE SI SYSTEM

ADRIAN CHUNG NING HANN

FACULTY OF ENGINEERING
UNIVERSITY OF MALAYA
KUALA LUMPUR

2021

# TITLE OF RESEARCH REPORT WHICH HAS BEEN APPROVED BY FACULTY OF ENGINEERING

**ADRIAN CHUNG NING HANN**

**RESEARCH REPORT IS SUBMITTED IN PARTIAL FULFILLMENT OF THE REQUIREMENTS FOR THE DEGREE OF MASTER OF MECHANICAL ENGINEERING**

**FACULTY OF ENGINEERING**
**UNIVERSITY OF MALAYA**
**KUALA LUMPUR**

**2021**

**UNIVERSITY OF MALAYA**

**ORIGINAL LITERARY WORK DECLARATION**

Name of Candidate: Adrian Chung Ning Hann

Registration/Matric No: KQK190006/17201235

Name of Degree: Master Degree of Mechanical Engineering

Title of Research Report (Study of Schottky and Poole-Frenkel Conduction Mechanism in Fe3O4-gamma-Fe2O3/SiO2/n-type Si System):

Field of Study:

I do solemnly and sincerely declare that:

(1) I am the sole author/writer of this Work;
(2) This Work is original;
(3) Any use of any work in which copyright exists was done by way of fair dealing and for permitted purposes and any excerpt or extract from, or reference to or reproduction of any copyright work has been disclosed expressly and sufficiently and the title of the Work and its authorship have been acknowledged in this Work;
(4) I do not have any actual knowledge nor do I ought reasonably to know that the making of this work constitutes an infringement of any copyright work;
(5) I hereby assign all and every right in the copyright to this Work to the University of Malaya ("UM"), who henceforth shall be owner of the copyright in this Work and that any reproduction or use in any form or by any means whatsoever is prohibited without the written consent of UM having been first had and obtained;
(6) I am fully aware that if in the course of making this Work, I have infringed any copyright whether intentionally or otherwise, I may be subject to legal action or any other action as may be determined by UM.

Candidate's Signature Date: 4/2/2021

Subscribed and solemnly declared before,

Witness's Signature Date: 4/2/2021

Name:

Designation:

## ABSTRACT

The advances of metal oxide semiconductor technology (MOS) have led to smaller devices being made where sizes of the devices keep getting smaller and compact. Hence, all the components of metal oxide semiconductor sizes are to be reduced without affecting the overall efficiency of the metal oxide semiconductor. However, there is a problem in the silicon dioxide component of MOS as the sizes of the silicon oxide ($SiO_2$) reduces, there is a possibility a current leakage to occur due to carrier direct tunneling effect passing through $SiO_2$ which reduce the efficiency of the MOS. Therefore, a higher dielectric constant material where $Fe_3O_4$-γ-$Fe_2O_3$/$SiO_2$/n-type (magnetite-maghemite nanoparticles with silicon dioxide) silicon system is chosen to tackle the problem. This material is to be study with the experiment data of the material in order to investigate the Schottky and Poole-Frenkel emission as well as to identify the dynamic dielectric constants of both emissions and barrier height of the Schottky emission of the material. The results show that the linear fitting of Schottky and Poole Frenkel emissions are well fitted with the standard model equations which suggested that both emissions are present during the experiment. Subsequently, the calculation and observation of the plotted graphs showed that the highest dynamic dielectric constant, $k_r$ of Schottky emission is 6.6927 at 200°C while the highest dynamic dielectric constant $k_r$ of Poole-Frenkel emission is 8.6505 at 150°C and the highest barrier height, $\Phi_B$ of Schottky emission is 1.6242 at 200°C. In conclusion, the overall results show that the combination of Schottky and Poole-Frenkel conduction mechanisms are responsible for the soft breakdown, $E_B$ of $Fe_3O_4$-γ-$Fe_2O_3$/$SiO_2$/n-type silicon system in a high electric field and high-temperature environment.

## ABSTRAK

Kemajuan teknologi semikonduktor logam oksida telah menyebabkan saiz peranti lebih kecil pembuatannya di mana saiz peranti terus menjadi semakin kecil dan padat. Oleh itu, semua komponen daripada semikonduktor oksida logam harus dikurangkan saiznya tanpa mempengaruhi kecekapan keseluruhan semikonduktor oksida logam. Walau bagaimanapun, terdapat masalah pada komponen silikon dioksida dalam semikonduktor logam oksida kerana apabila ketebalan silikon oksida ($SiO_2$) dikurangkan, kemungkinan berlakunya kebocoran arus disebabkan oleh kesan pembawa terowong langsung yang melalui $SiO_2$ yang mengurangkan kecekapan teknologi semikonduktor logam. Oleh itu, bahan pemalar dielektrik yang lebih tinggi seperti sistem silikon $Fe_3O_4$-$\gamma$-$Fe_2O_3$/$SiO_2$/jenis-n (magnetit-maghemite dengan silikon dioksida) diperlukan dan dipilih untuk mengatasi masalah tersebut. Bahan tersebut telah dikaji dengan data eksperimen untuk menyiasat pelepasan Schottky dan Poole-Frenkel serta untuk mengenal pasti pemalar dielektrik dinamik kedua-dua pelepasan tersebut dan ketinggian penghalang pelepasan Schottky. Hasil kajian menunjukkan bahawa regresi linear pelepasan Schottky dan Poole Frenkel adalah sangat sesuai dengan persamaan model standard dan secara langsung menunjukkan bahawa kedua-dua pelepasan tersebut hadir semasa eksperimen berlangsung. Kemudian, hasil pengiraan dan pemerhatian pada graf menunjukkan bahawa pemalar dielektrik dinamik tertinggi, $k_r$ pelepasan Schottky adalah 6.6927 pada 200°C manakala pemalar dielektrik dinamik tertinggi, $k_r$ pelepasan Poole-Frenkel adalah 8.6505 pada 150°C dan penghalang tertinggi tinggi, $\Phi_B$ pelepasan Schottky ialah 1.6242 pada 200°C. Kesimpulannya, hasil keseluruhan dari analisa data eksperimen dan graf menunjukkan bahawa kombinasi mekanisme konduksi Schottky dan Poole-Frenkel bertanggungjawab dalam pemecahan lembut, $E_B$ yang berlaku dalam sistem silikon jenis $Fe_3O_4$-$\gamma$-$Fe_2O_3$/$SiO_2$/jenis-n pada medan elektrik dan persekitaran suhu yang tinggi.

## ACKNOWLEDGEMENTS

First and foremost, I would like to express my deep and sincere gratitude to my supervisor, Associate Professor Ir. Dr. Wong Yew Hoong, for giving me the opportunity to do research and provide invaluable guidance throughout this research project. It was a great privilege and honor to learn under his tutelage. I am eternally grateful for his teaching.

Next, I would like to express my utmost gratitude to my father and especially my brother. My brother has taught me the fundamentals of research in which he has experience and knowledge throughout his study previously. For that, I am utterly thankful for the support as a family member and as a fellow researcher.

Last but not least, I would like to express my thanks to my course mates, friends, and all those who contribute either directly or indirectly to the process of the research report. For my course mates, you have my deepest gratitude for the time we had been together for the last two semesters.

## TABLE OF CONTENTS

## LIST OF FIGURES

## LIST OF TABLES

## LIST OF SYMBOLS AND ABBREVIATIONS

| | | |
|---|---|---|
| $\mu$ | : | Electronic mobility in oxide |
| $A^*$ | : | Richardson constant |
| Al | : | Aluminum |
| $C$ | : | Intercept of the graph |
| $CeO_2$ | : | Cerium oxide |
| $Dy_2O_3$ | : | Dysprosium oxide |
| $E$ | : | Electric field |
| $E_B$ | : | Soft breakdown |
| $\varepsilon_0$ | : | Permittivity of the vacuum |
| $Fe^{2+}$ | : | Ferrous ion |
| $Fe^{3+}$ | : | Ferric ion |
| $Fe_3O_4$ | : | Magnetite |
| FN | : | Fowler-Nordheim |
| FNP | : | Functionalized nanoparticle |
| $h$ | : | Planck constant |
| $HfO_2$ | : | Hafnium (IV) oxide |
| $J$ | : | Current density |
| $J_{FN}$ | : | Current density of Fowler-Nordheim |
| $J_{Ohm}$ | : | Current density of Ohm's law |
| $J_{PF}$ | : | Current density of Poole-Frenkel |
| $J_{SE}$ | : | Current density of Schottky Emission |
| $J_{TFL}$ | : | Current density of Trap-filled-limit conduction |
| $k$ | : | Boltzmann constant |
| $k_r$ | : | Dielectric constant |

| | | |
|---|---|---|
| $m$ | : | Free electron mass |
| $m^*$ | : | Effective electron mass |
| MOS | : | Metal oxide semiconductor |
| MOSFET | : | Metal oxide semiconductor field transistor |
| $m_{ox}$ | : | Effective electron mass of oxide |
| MRI | : | Magnetic resonance imaging |
| n | : | Refractive index |
| $N_2$ | : | Nitrogen gas |
| $N_c$ | : | State density of the conduction band |
| $NH_4OH$ | : | Ammonium hydroxide |
| $n_o$ | : | Thermal equilibrium of the concentrated free charge carriers |
| N-type | : | Negative type |
| $Pr_2O_3$ | : | Praseodymium (III) oxide |
| $P_t$ | : | Platinum |
| P-type | : | Positive type |
| $q$ | : | Electronic charge |
| $R^2$ | : | Statistical measure of linear regression |
| RRAM | : | Resistive random-access memory |
| S | : | Gradient of the slope |
| SCLC | : | Space-Charge-Limited Conduction |
| Si | : | Silicon |
| SiC | : | Silicon carbide |
| $SiO_2$ | : | Silicon dioxide |
| SiON | : | Silicon Oxynitride |
| $SnO_2$ | : | Tin oxide |
| S-OH | : | Silicon hydroxide |

| | | |
|---|---|---|
| $T$ | : | Absolute temperature |
| $T_c$ | : | Characteristic temperature of trap distribution |
| TFL | : | Trap-filled-limit |
| $t_{ox}$ | : | Thickness of the oxide or interfacial layer |
| $V$ | : | Voltage |
| $V_g$ | : | Surface potential of Si at a specific gate voltage |
| $ZrO_2$ | : | Zirconium oxide |
| $\alpha$-$Fe_2O_3$ | : | Hematite |
| $\beta$-$Ga_2O_3$ | : | Germanium based metal oxide |
| $\gamma$-$Fe_2O_3$ | : | Maghemite |
| $\Phi_B$ | : | Barrier height |
| $\Phi_t$ | : | State density of the trap energy |

# CHAPTER 1: INTRODUCTION

The advancement for metal oxide semiconductor technology has enabled more miniaturization of semiconductor devices such as chips, diodes, transistors, etc. Consequently, the size of a metal oxide semiconductor has to be reduced correspondingly without affecting its electrical capability. Therefore, a material that is used as a gate dielectric (insulator) in a metal oxide semiconductor known as $SiO_2$ (silicon dioxide) has to be reduced in size as well. However, there is a problem that occurred in the reduction of the size of $SiO_2$. As the sizes of the $SiO_2$ are reduced, there is a possibility of current leakage increases due to direct tunneling of carriers through $SiO_2$ (Robertson, 2004; Wong, 2010). Hence, a higher dielectric constant ($k_r$) oxide material is required as an alternative dielectric to substitute $SiO_2$.

For this study, iron oxide particles which consist of magnetite-maghemite ($Fe_3O_4$-γ-$Fe_2O_3$) nanoparticles are to synthesize with 4-pentynoic acid and to be self-assembled on silicon dioxide to detect its dielectric properties for replacement of silicon dioxide. In this project, the research of the higher dielectric constant oxide material using magnetite-maghemite nanoparticles are to be studied by using high conduction mechanism studies such as Schottky and Poole-Frenkel emission mechanisms.

## 1.1 Objective

The objectives for this research project are crucial to determine the important criteria and variables that are mainly studied and analyzed in this research. Data will be obtained through experimentation and reference from the researchers A. A. Baharuddin, Ang, B.C., Wong, Y.H. (2017) in which to analyze and computed using certain parameters to fulfill the current objectives. The main focus of the study of the conduction mechanisms in this research is Schottky and Poole-Frenkel emission. The objectives for the research project are:

1. To investigate the Schottky and Poole-Frenkel emission mechanisms in $Fe_3O_4$-gamma-$Fe_2O_3$/$SiO_2$/n-type Si System.
2. To compute and compare the dynamic dielectric constants, $k_r$ in the oxynitride material caused by Schottky and Poole-Frenkel emission mechanisms in $Fe_3O_4$-gamma-$Fe_2O_3$/$SiO_2$/n-type Si System.

# CHAPTER 2: LITERATURE REVIEW

## 2.1 Introduction

Research is conducted to comprehend the basic mechanism of gate dielectric material in MOS (metal oxide semiconductor). The current development of technology has been focusing on reducing the size of the chip which causes the MOS size to be reduced (Bersch, 2008). However, the smaller size of MOS will indirectly affect the current leakage issue in the gate dielectric since the standard $SiO_2$ (silicon dioxide) material as the gate dielectric are unsusceptible due to size reduction. Alternatively, this problem could be avoided by having a high dielectric constant ($k_r$) oxide where the size reduction will not be an issue as a replacement of dielectric material.

Detailed explanation and elaboration of the dielectric constant with its susceptibility to thermal changes that will cause the leakage in the material will be discussed in the literature review section. In this project, the Schottky and Poole-Frenkel emission mechanisms are the primary focus to understand the high conduction current mechanism of the MOS. Various research and studies that were conducted before will be analyzed and reviewed throughout the literature review chapter.

## 2.2 Metal Oxide Semiconductor (MOS)

### 2.2.1 History of Metal Oxide Semiconductor (MOS)

A metal-oxide-semiconductor is a semiconductor device in which a type of metallic oxide such as silicon dioxide serves as an insulating layer between the semiconductor (Incorporated, 2020). The attempt to establish and perfecting metal oxide semiconductors to become one of the integral parts of the electronic device began nearly 70 years ago. There are few independent efforts in establishing the field-effect principle which later becomes the working principle for metal oxide semiconductors during the 1930s (Sah, 1964).

At the end of 1947, Barden and Brattain discovered the transistor effect and established the point-contact transistor (Arns, 1998; Sah, 1964). However, few problems arise for researchers in developing field-effect and one of the problems lies in semiconductor surfaces that cause the field-effect transistor to not work (Arns, 1998; Sah, 1964). Although a Bell Laboratories researcher manages to find the solution to solve these problems in 1958 (Arns, 1998), researchers at that time are not interested in the pursuit of developing a field-effect transistor.

Nevertheless, the interest in metal-oxide-semiconductor field-effect transistor was reignited by Kahng (1960) by presenting the first successful silicon inversion-channel MOSFET in 1960 (Liou, 1998). After that, during the 1970s and 1980s, metal oxide semiconductor was developed and widely used in forming integrated circuits as a metal oxide semiconductor is fundamentally simpler in comparison to other transistor and could be packed on a single chip (Arns, 1998; Liou, 1998). Since then, metal oxide semiconductors had revolutionized the electronics industry which makes it to become one of the integral parts of most current electronic devices.

### 2.2.2 Fundamental of Metal Oxide Semiconductor (MOS)

The name of a metal oxide semiconductor (MOS) is referring to a metal gate, oxide interface, and semiconductor mostly silicon based. However, the metal part of MOS can be replaced by a layer of polysilicon (polycrystalline silicon) (Murray A.F., 1987). MOS structure is a type of sandwich structure in which a thin layer of silicon dioxide is placed in the middle between the semiconductor and metal layer (Murray A.F., 1987; Xuan, 2020). These three layers are also known as drain (silicon), channel (silicon dioxide), and source (metal) which work as diodes and connect in series back-to-back (Murray A.F., 1987). Figure 2.1 shows a schematic of an ideal metal oxide semiconductor device.

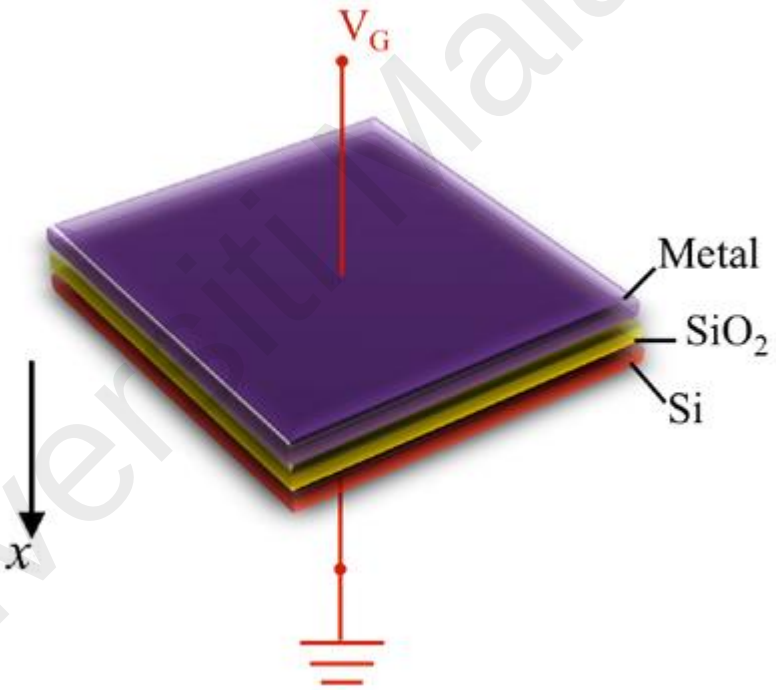


Figure 2.1: A Schematic of an Ideal Metal Oxide Semiconductor Device (Xuan, 2020)

There are few general properties of a metal oxide semiconductor (MOS) that should be noted below in which as follows (Xuan, 2020):

1. The oxides layer in the middle which in this case is the $SiO_2$ should be a perfect insulator with zero current flowing through under all static biasing settings.
2. The semiconductor should be uniformly doped with acceptors or donors as n-type or p-type semiconductors.
3. The silicon layer which is the semiconductor should be large enough for charges to encounter a field-free region known as silicon bulk before reaching the back contact.
4. The Ohmic contacts should be initiated on the backside of the metal oxide semiconductor devices.
5. The metallic gate should be large enough to be an equipotential region.

In most applications, MOS is used as a switching device. This is made possible as the density of charge carriers in the semiconductor near the silicon dioxide interface can be controlled by the voltage applied to the gate (Bersch, 2008). As the voltage is applied between the body and gate terminals, the electric field produced penetrates through the oxide and creates a transposition layer or channel in which current can pass between source and drain terminals (Murray A.F., 1987).

This phenomenon also can be referred to as electron-hole pair (Murray A.F., 1987) as the electron (current) jump across this channel as the hole generated at the silicon which is due to the excitation of the electron at the metal end by the applied voltage. By varying the voltage between the gate and body, the conductivity of the channel can be regulated and thereby controls the current flow between the source and drain (Murray A.F., 1987). There are two types of metal oxide semiconductors which are n-type and p-type semiconductors. Both types of semiconductors are shown as an illustration in figure 2.2 below where D is referred to as the drain, G is the gate and S is the source.

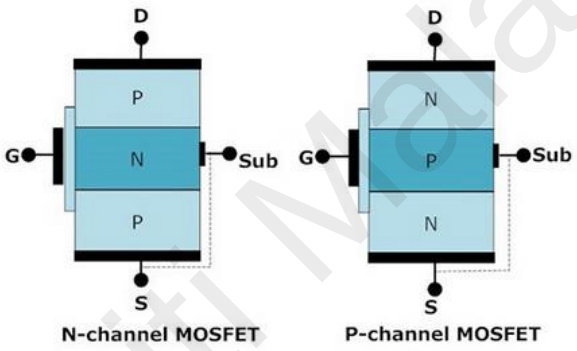


Figure 2.2: N-Type and P-Type Metal Oxide Semiconductor (Electronicshub.Org, 2020)

The difference between n-type and p-type semiconductor can change the way of metal oxide semiconductor operation. Therefore, it is crucial to understand the significance of the difference between both types of semiconductors. For this research, an n-type semiconductor is chosen as the testing parameter. The difference between n-type and p-type semiconductor can be further elaborated in Table 2.1 below.

Table 2.1: Difference of N-Type and P-Type Semiconductor (Globe, 2020)

| Type of Semiconductor | N-Type Semiconductor | P-Type Semiconductor |
|---|---|---|
| Elements of Periodic Table in Doping Element | V Group Element | III Group Element |
| Nature of The Doping Element | Added impurity bestow extra electrons and called as Donor Atom | Added impurity produces vacancy of the electron (holes) known as Acceptor Atom |
| Type of Added Impurity | Phosphorous, Arsenic, Antimony, Bismuth, etc. | Aluminum, Gallium, Indium, etc. |
| Majority Carriers | Electrons | Holes |
| Minority Carriers | Holes | Electrons |
| Density of Holes and Electrons | Electrons greater than holes | Holes greater than electrons |
| Level of Energy | Donor energy level is away from the valence band and closer to the conduction band | Acceptor energy level is away from the conduction band and closer to the valence band |
| Level of Fermi | Fermi level situated between donor energy and conduction band | Fermi level situated between acceptor energy and valence band |
| Movement of Majority Carriers | Lower to higher potential | Higher to lower potential |

## 2.3 High Dielectric Constant Material

### 2.3.1 Silicon Dioxide

Silicon dioxide ($SiO_2$) is also commonly known as silica, is a natural compound that consists of silicon and oxygen which could be found abundantly in the sand (Information, 2020). Silica has three main types of crystalline varieties which are quartz, tridymite, and cristobalite (Information, 2020). Silica or silicon dioxide compounds can be separated into two groups which are crystalline and amorphous silica (Information, 2020). Amorphous silica or silicon dioxide is used as dielectric or insulators in transistors, capacitors, and metal oxide semiconductors where it can function to insulate multiple electronic elements and as a sacrificial or structural layer in various micromachining process (Reed & Fedder, 1998). Silicon dioxide ($SiO_2$) had been used as a gate dielectric and insulator in metal oxide semiconductor (MOS) devices and structures for years (Eranen, 2010; Wong, 2010).

Silicon stands out among others where silicon is a vital material in modern semiconductor mechanics and always has been chosen for the application of low-power devices (Deniz, 2013). Moreover, silicon is also used in metal oxide semiconductors (MOS) in major capacitor structures since they formed the foundation of the MOS field-effect transistor (Neamen, 2012). Silicon is able to grow its oxide which is silicon dioxide ($SiO_2$) under thermal conditions where it works as an effective insulator for capacitors (A. A. Baharuddin, Ang, B.C., Wong, Y.H., 2017). Nevertheless, while silicon dioxide growth may be improved to create a defect-free boundary with silicon, the surfaces of silicon dioxide would be less defined which would cause a disadvantageous situation (Li, 2016). There are possibilities of surfaces of silicon dioxide hydrogenated to become silicon hydroxide (S-OH) defects and could contain water which could lead to issues such as hysteresis and interface trapping (Miozzo, 2010). Therefore, in order to eliminate these drawbacks, the self-assembly of an organic compound can be a significant solution.

In this project, silicon dioxide is chosen as the main focus in researching better dielectric material in metal oxide semiconductor devices as the reduction of sizes plays a vital role in integrated circuits. The latest development on the miniaturization of MOS devices causes the sizes of the gate dielectric of silicon dioxide had to be reduced as well. However, once the oxide thickness is less than 1.2 nm, the possibility of current leakage issue cause by the direct tunneling of carriers through $SiO_2$ is imminent (Robertson, 2004; Wong, 2010). In order to tackle this issue, there is a need to replace the standard $SiO_2$ material with a higher dielectric constant oxide material. The high dielectric constant oxide material must be able to withstand the size reduction with low current leakage and able to withstand high temperature.

### 2.3.2 Iron Oxide – Magnetite-Maghemite ($Fe_3O_4$-γ-$Fe_2O_3$) Nanoparticles

Iron oxide nanoparticles are known to be used in applications such as catalysis, high-density data storage, magnetic resonance imaging (MRI), hyperthermia applications, drug delivery facilitators, bioprocessing, supercapacitors, and ferrofluids (Ghosh, 2014; Goswami, 2016; Hosseini-Monfared, 2015; Nemethova, 2017; Sun, 2006; Terris, 2005). There are three types of derivatives for iron oxide particles which are maghemite (γ-$Fe_2O_3$), magnetite ($Fe_3O_4$), and hematite (α-$Fe_2O_3$) (A. A. Baharuddin, 2017). As different phases of iron oxide nanoparticles will lead to discrete properties for multiple applications, it is important in synthesizing iron oxide nanoparticles into specific particle sizes, distribution of sizes, customized particle geometry, and distinct morphology in the nanomaterials field (Li, 2016).

Nanoparticles such as iron oxide have an extremely high inclination of aggregation and adhesion compared to sub-micron sized particles. As such, it is vital to develop techniques to regulate the aggregation/dispersion of nanoparticle phenomena to apply to functional products and materials in industrial applications (Pichon, 2012). Magnetite ($Fe_3O_4$) is the most researched material among the iron oxides due to its superparamagnetic behavior with high magnetization saturation at ambient temperature in which electron delocalization could take place between the adjoining site of both $Fe^{2+}$ and $Fe^{3+}$ (Lu, 2007). Furthermore, its high biocompatibility and non-toxicity make it logical to be selected and applied in various applications in particular biotechnology areas. Magnetite has a black ferrimagnetic mineral which consists of Fe (II) and Fe (III) elements where the material is often non-stoichiometric and exhibited cation defective Fe (III) layer (A. A. Baharuddin, Ang, B.C., Wong, Y.H., 2017).

Magnetite possesses an inverse spinel crystal structure that consisted of a unit cell of 32 oxygen atoms in a face-centered cubic (FCC) structure (A. A. Baharuddin, Ang, B.C., Wong, Y.H., 2017). The half-metallic properties of magnetite have made it a fascinating material to be applied in spin electronics applications. However, magnetite is unstable in oxidizing conditions and known to transmute into maghemite ($\gamma$-$Fe_2O_3$) and hematite ($\alpha$-$Fe_2O_3$) as temperature increases (De Faria, 1997; Lu, 2007). Hence, the synchronization of magnetite-maghemite ($Fe_3O_4$-$\gamma$-$Fe_2O_3$) able to occur more frequently (S. R. Chowdhury, Yanful, E.K., 2010, 2013; S. R. Chowdhury, Yanful, E.K., Pratt, A.R., 2012; S. Kim, Surek, J., Baker-Jarvis, J., Provenzano, V. , 2012). Nevertheless, hematite can be reversible to magnetite through the reduction of hydrogen (Pang, 2016).

Magnetite is conductive at ambient temperature causes by a hopping mechanism (A. A. Baharuddin, 2017). Magnetite has a relatively large theoretical lithium storage capacity and the ability to function as highly pseudocapacitive material via redox reactions (Ma, 2015). To date, magnetite has been under the spotlight in the development of electrochemical conversion devices and energy storage as a reaction toward progressive depletion of fossil fuel and environmental quality degradation (Li, 2016).

The studies of iron oxide in thin-film form and the application of the thin film in metal oxide semiconductor are not yet fully developed due to the constraints such as their complicated crystal structure with large unit cell and numerous unfilled interstitial sites. The bulk properties of iron oxide thin film are attractive, but it is hard to be attained (Cibert, 2005). The transport and magnetic properties of iron oxide are greatly influenced by the distribution of the $Fe^{2+}$ and $Fe^{3+}$ ions in the tetrahedral and octahedral areas (A. A. Baharuddin, 2017). This causes the properties of iron oxide thin film to changes notably from the bulk and depends greatly on the deposition technique during forming on the substrate. It was confirmed that the actual thin film of magnetite is able to have spin polarization similar to ferromagnetic metals (Cibert, 2005).

Based on the literature, iron oxide nanoparticles are chosen as the ingredient for the functionalized nanoparticle to be synthesized with silicon dioxide in order to test the significance of the material especially in electrical characterizations of the functionalized iron oxide nanoparticles on silicon dioxide structure.

## 2.4 Charge Conduction Mechanism on High Dielectric Constant Materials

The main purpose of this research project is to understand the influence and effect of magnetite-maghemite nanoparticles on silicon dioxide/n-type silicon substrate. The study of leakage characteristics is one of the important aspects of electrical properties for high dielectric constant material in metal oxide semiconductor devices. Therefore, it should be closely studied based on the comprehension of the workings of charge conduction mechanisms. The literature review in this chapter is based on the charge conduction mechanisms that are used to understand the leakage characteristics of the material that are related to this research project.

### 2.4.1 Oxide Breakdown

Enough large electrical field applied to the oxide layer could lead to oxide breakdown that would ultimately cause disastrous failure and huge leakage to occur. The defects of the oxide also could lower the breakdown field and lead to oxide breakdown. The tunneling phenomena of the high electric field that causes thin oxide to breakdown is also referred to as Fowler-Nordheim (FN) tunneling (Ravindra, 1992).

The tunneling effect later resulted in a large density of electrons to constrict to a constricted potential well at the interface (Ravindra, 1992). This then causes the energy quantization to the interface and causes the energy levels to separate into two sources of energy emission that eventually leads to Fowler-Nordheim tunneling (Ravindra, 1992). In order to prevent oxide breakdown, a safety margin is necessary when estimating appropriate gate voltage with the thickness of the oxide in metal oxide semiconductor (Neamen, 2012).

The leakage current density-electric field (J-E) is required to understand the leakage and oxide breakdown characteristics of any high dielectric constant materials. The J-E measurement is obtained and transformed from the current-voltage (I-V) measurement of the high dielectric constant material (A. A. Baharuddin, 2017). In order to redress contact with an n-type semiconductor, an electron was permitted to be moved over the potential barrier (Neamen, 2012). The barrier height, $\Phi_B$ is the band edge conduction between the interfacial layer of oxide and silicon that can be obtained from the Fowler-Nordheim (FN) tunneling model (A. A. Baharuddin, 2017).

The J (electric field) assigned to Fowler-Nordheim tunneling ($J_{FN}$) is shown in the equations below (Schroder, 2006):

$$J_{FN} = AE^2 \exp(-B/E) \tag{2.1}$$

Where,

$$A = \frac{\left(\frac{q^3}{8\pi\Phi_B}\right)}{\frac{m}{m_{ox}}} \tag{2.2}$$

And,

$$B = \frac{\left[8\pi(2m_{ox}\Phi_B^3)^{1/2}\right]}{3qh} \tag{2.3}$$

Where $h$ is the Planck constant ($4.135 \times 10^{-15}$eV s), $m_{ox}$ is known as effective electron mass in the oxidized layer, $m$ is known as free electron mass. By substituting all the constants into equations 2.4 and 2.5 gives:

$$A = 1.54 \times 10^{-6}(m/m_{ox}\Phi_B) \tag{2.4}$$

Where $m/m_{ox}$ is assumed to be 0.3, and

$$B = 6.83 \times 10^{7}(m_{ox}\Phi_B^3/m)^{1/2} \tag{2.5}$$

By rearranging equation 2.1 with the values of constant from equations 2.4 and 2.5 yields:

$$\ln(J_{FN}/E^2) = \ln(A) - B/E \tag{2.6}$$

Equation 2.4 is a definition of a linear equation that is attributed to the Fowler-Nordheim tunneling model where the graph of Fowler-Nordheim tunneling can be plotted where $\ln(J_{FN}/E^2)$ is the y-axis variable, 1/E is the axis-variable, B is the gradient of the graph ,and ln(A) is the y-intercept. Through substitution of the y-intercept and the gradient will yield the barrier height from the Fowler-Nordheim tunneling graph which will be explained more thoroughly in the results and discussion section.

### 2.4.2 Schottky Emission (SE)

Schottky emission also is known as thermionic emission is a conduction mechanism where electrons are able to obtain enough energy due to thermal activation or rising of temperature by application of electric field (voltage) to pass through over a surface barrier (Britannica, 2016; Cheong, 2008; F-C. Chiu, 2014). This phenomenon enables the electrons to overwhelm the energy barrier of the dielectric material and causes the electrons to discharge over the energy barrier from the surface of the dielectric material (Britannica, 2016; F-C. Chiu, 2014).

Meanwhile, at the same time, the Schottky effect occurs in parallel with the emission where the energy barrier height of the dielectric material could be lowered by image force and application of electric field (Chiu, 2014). At extreme values of the applied field, the electron emission experiences an enormous increase due to another type of emission known as high-field emission or simply known as field emission (Britannica, 2016). The effect and emission phenomenon were discovered by a German physicist, Walter Schottky where the effect and emission were named after him (Britannica, 2016).

There are numerous studies conducted by the researchers to understand and investigate the Schottky emission and its effect on various types of materials that are related to high dielectric constant materials. The Schottky emission and effects studies will be highlighted in this literature reviews to showcase some of the efforts of the researchers to understand the very impact of this phenomenon toward the development of metal oxide semiconductor.

The research of Schottky emission began as early as in 1962, where Emtage (1962) conducted the research of the Schottky emission through thin insulating films which is the polymerized silicon oil on a gold film. The results showed that there are two ways of estimating metal-insulator work functions which are the observed values of α and temperature dependence of the current (Emtage, 1962). This research signaling the beginning of the extensive investigation and study regarding Schottky emission towards high dielectric materials.

In another research conducted by (Zafar, 1998), the study of Schottky conduction mechanism in barium strontium titanate thin films leads to inconsistent Richardson and dielectric constants with their experiment values. They are able to resolve the difficulties associated with the standard Schottky equation with modified Schottky equation and able to provide results of barrier height and dielectric constants on barium strontium titanate films (Zafar, 1998). There is one condition in order to apply the modified Schottky equation according to Simmons's theory where the electronic mean free path in the insulator is less than the film thickness (Simmons, 1965).

Chiu with his fellow researchers conducted multiple studies on Schottky and Poole-Frenkel's charge conduction mechanism with various types of materials and the results observed enable researchers to understand the concept of the conduction mechanisms on materials. F.-C. Chiu, Lin, Z-H., Chang, C-W., Wang, C-C., Chuang, K-F., Huang, C-Y., Lee, J. Y-M., Hwang, H-L. (2005) conducted an electron conduction mechanism study on sputter-deposited Al/$ZrO_2$/Si structure where electrical properties and essential structures of zirconium oxide ($ZrO_2$) thin films were studied. The results show that the predominant conduction mechanism at high temperatures was Schottky emission in a high electric field and modified Schottky emission in a medium electric field (F.-C. Chiu, Lin, Z-H., Chang, C-W., Wang, C-C., Chuang, K-F., Huang, C-Y., Lee, J. Y-M., Hwang, H-L., 2005). Moreover, it also determined that the trap energy level and barrier height of Al/$ZrO_2$ were 1.1 eV and 0.92 eV respectively (F.-C. Chiu, Lin, Z-H., Chang, C-W., Wang, C-C., Chuang, K-F., Huang, C-Y., Lee, J. Y-M., Hwang, H-L., 2005).

After that, Chiu published articles regarding the study of Schottky emission in metal/hafnium oxide ($HfO_2$)/silicon structure and metal/dysprosium oxide ($Dy_2O_3$)/silicon structure where structural and electrical characterization with comparisons between the materials were being made and evaluated (F-C. Chiu, 2006, 2007). The results determined that Schottky emission in metal/HfO2/silicon is dominant in high temperature and the barrier height of $HfO_2$ was determine using the mathematical iteration method to be 0.94 eV (F-C. Chiu, 2006). Meanwhile, the charge conduction mechanism that was dominant in metal/$Dy_2O_3$/silicon were the Schottky emission from 300 to 325 K and space-charge-limited mechanism from 350 to 525 (F-C. Chiu, 2007). In 2010, Chiu and Lai conducted electrical and optical characterizations on cerium oxide ($CeO_2$) thin films. The experimental results showed that the electrical conduction mechanism that occurs from 350 to 500 K were determined to be Schottky emission in a medium electric field (F.-C. L. Chiu, C-M. , 2010).

In 2008, Cheong and his fellow researchers studied and investigated the current conduction mechanisms that occurred within atomic-layer-deposited $HfO_2$/nitrided where different thicknesses were stacked on thick nitrided $SiO_2$. They discovered that Schottky emission is one of the dominant conduction mechanisms in pure $HfO_2$ samples (Cheong, 2008). However, Schottky emission was not been recognized as the dominant conduction mechanism in impure $HfO_2$ samples (Cheong, 2008). Furthermore, another research was conducted that involved $HfO_2$ film in Al/$HfO_2$/p-Si metal oxide semiconductor (MOS) structure at different temperatures ranging in between 320 and 100 K in order to discover the structure's current conduction mechanism (Pakma, 2012). The schematic diagram of Al/$HfO_2$/p-Si MOS structure can be seen in figure 2.3.

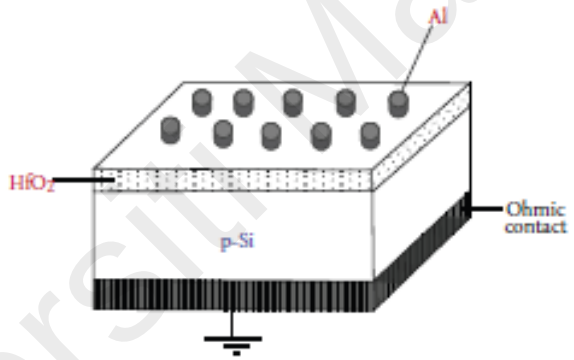


Figure 2.3: Schematic Diagram of Al/$HfO_2$/p-Si MOS Structure (Pakma, 2012)

The *J-V* (current density-voltage) measurement showed that Schottky emission was compatible at the temperature between 100 and 320 K (Pakma, 2012). Then, the Schottky emission was used to determine the structure's refractive index values, barrier heights, and dielectric constants of the $HfO_2$ thin films. In the results reported in the article, the refractive index values and dielectric constant were noted to decrease as temperature decreases (Pakma, 2012). The barrier height at the Al/$HfO_2$ and $HfO_2$/p-Si interfaces was calculated as 0.936 and 0.778 eV (320 K) to 0.482 and 0.42 eV (100 K) respectively (Pakma, 2012).

Meanwhile, in another research, Wong (2011) studied and published the electrical characteristics of oxidized/nitrided zirconium thin film in silicon. This study was conducted to determine whether a new method of deposition which is the simultaneously oxidized and nitrided sputtered of zirconium thin film on silicon could bring a better high dielectric constant material (Wong, 2011). The experimental results showed that hard oxide breakdown occurred at the higher electric field due to the combination of Poole-Frenkel emission, Schottky emission, and Fowler-Nordheim tunneling (Wong, 2011).

Another researcher conducted a study on Schottky emission on gadolinium doped $SiO_2$ thin films for resistive random-access memory (RRAM) devices (Chen, 2018). The results were observed that the Schottky distance trend of the RRAM devices was continuously increased and resulted in large exhaustion of electrons transmission in an oxygen-filled environment in compared to a vacuum environment (Chen, 2018).

Furthermore, researchers in Greece conducted research on a germanium-based metal oxide semiconductor ($Ni/HfO_2/\beta\text{-}Ga_2O_3$) in comparison to the standard usage of a silicon-based metal oxide semiconductor (Botzakaki, 2020). The research showed that the Schottky conduction mechanism occurs in high applied bias voltages and high temperatures (Botzakaki, 2020). The barrier heights of $Al/HfO_2$ interfaces and $HfO_2$/p-Ge were evaluated to be 1.3 ± 0.2 eV and 1.7 ± 0.2 eV respectively (Botzakaki, 2020). Meanwhile, the researchers also able to determine Poole-Frenkel emission which was dominant within the voltage range of 0.4-1.5 V where the trap energy level of $HfO_2$ films was calculated to be $\varphi t = 0.36$ eV (Botzakaki, 2020).

Another research used different gamma irradiation doses on gallium metal oxide semiconductors (MOS) to determine the changes and effect of gamma irradiation on the conduction mechanism of MOS (Manikanthababu, 2020). The Schottky emission mechanism appeared as the governing conduction mechanism in the in-between 1 kGy to 200 kGy doses while the Poole-Frenkel emission mechanism appeared dominant when the dose increases to 200 kGy (Manikanthababu, 2020). The barrier heights were extracted using Schottky emission for the pristine was around 0.95 to 0.83 eV (Manikanthababu, 2020).

To sum up, researchers conducted on Schottky emission studies were done in order to understand the relationship of charge conduction mechanism associate with high temperature that occurs in between metal and oxide interface. Through the usage of Schottky emission and theory to an extent, it helped other researchers to understand further the significance of the phenomenon that often occurs to most high dielectric constant materials and able to improve the functionality of those materials that are important in the structure of metal oxide semiconductor.

### 2.4.3 Poole-Frenkel Emission (P-F)

Poole-Frenkel emission has a similar mechanism as Schottky emission where electrons experiencing thermal excitation may transfer from the traps into the dielectric conduction band (F-C. Chiu, 2014). Hence, Poole-Frenkel emission is sometimes also known as internal Schottky emission. Poole-Frenkel emission is one of the examples of a bulk-limited conduction mechanism where the emission of electrons happens within the bulk of the dielectric material. This phenomenon is caused when an applied electric field over the dielectric film reducing the Coulomb potential electron energy where the electrons are situated in the trapping center (bulk oxide) (F-C. Chiu, 2014; Wong, 2011). The reduction of potential energy increases the chances of an electron to be thermally excited from the trap into the dielectric conduction band (F-C. Chiu, 2014). Originally, Poole-Frenkel emission was discovered and published by Yakov Frenkel in 1938 from the extension theory that earlier developed by H.H. Poole (Connell, 1972; Dhariwal, 1989).

There are countless studies conducted by various researchers in studying and exploring the Poole-Frenkel emission and its effect with multiple types of materials that are related to high dielectric constant materials. The Poole-Frenkel emission and effects studies will be highlighted in this literature reviews to present some of the endeavors of the researchers to recognize the very influence of this phenomenon toward the development of metal oxide semiconductor.

There is research conducted in 2004 to determine the conduction and trapping mechanisms of $SiO_2$ films where the $SiO_2$ films were formed using multipolar electron cyclotron resonance with enhanced chemical vapor deposition also known as (ECR PECVD) (Isai, 2004). There are few conditions for the $SiO_2$ layer to become an excellent gate dielectric for metal oxide semiconductors and transistors where the $SiO_2$ layer has to contain low trapping probability, high breakdown field, low interface trap density, resistance to electrical stress, and high oxide integrity (Isai, 2004). The results of the experiment showed that leakage current observed from the experiment are a combination of Poole-Frenkel and Fowler-Nordheim current for numerous temperatures (Isai, 2004). The electrons that were trapped in the bulk of the oxide during electrical stress were found to be available at the interface which depending on the value of the electric field (Isai, 2004).

Moreover, another type of Poole-Frenkel conduction mechanism such as tunneling assisted Poole-Frenkel conduction mechanism was also used in studying the electrical characteristic behavior of $HfO_2$ thin films in a $Pt/HfO_2/Si$ capacitor (Jeong, 2005). Tunneling assisted Poole-Frenkel conduction mechanism can be described as electron tunneling from an electrode of metal that traps in a close-by insulator layer followed by the release of trapped electrons from the traps due to an applied electric field which lowered the potential well (Jeong, 2005).

The research results from the current density versus applied electric field graph showed that there a similarity of electric-field dependency to the Poole-Frenkel emission (Jeong, 2005). However, unlike Poole-Frenkel emission, the activation energy that contributed to the leakage current density in this experiment was correlated more to the Schottky barrier height value (Jeong, 2005). Therefore, tunneling assisted Poole-Frenkel conduction mechanism was able to explain the electrical transport better due to the insulating films consist of high trap density and the contacts contain blocking nature (Jeong, 2005).

As mentioned in the Schottky emission chapter, Chiu and his fellow researchers also conducted research on various electrical conduction mechanisms, in particular, Schottky and Poole-Frenkel emission. In this chapter, the Poole-Frenkel emission will be the main focus in highlighting the works of Chiu and his fellow researchers. In the research of electron conduction mechanism on sputter-deposited on zirconium oxide in Al/$ZrO_2$/Si, the results showed that Poole-Frenkel emission was dominant in high temperature (>425 K) with high electric fields (F.-C. Chiu, Lin, Z-H., Chang, C-W., Wang, C-C., Chuang, K-F., Huang, C-Y., Lee, J. Y-M., Hwang, H-L., 2005). Meanwhile, another research on $Pr_2O_3$/oxynitride in Al/$Pr_2O_3$/SiON/n-Si metal oxide semiconductor showed that Poole-Frenkel emission was the leading conduction mechanism in a high electric field (>2 MV/cm) that occur in the experiment and the trap energy level observed from Arhenius plot was around 0.56 ± 0.01 eV (F.-C. Chiu, Lee, C-Y., Pan, T-M. , 2009). In addition, Chiu and Lai also conducting electrical characterization on cerium oxide thin films where they detected Poole-Frenkel emission in a high electric field (> 2.36 MV/cm) from the temperature of 450 to 500 K (F.-C. L. Chiu, C-M. , 2010).

In 2010, research was conducted on experimental analysis of the Poole-Frenkel mechanism on thermally grown silicon dioxide with thick epitaxial 4H-SiC (silicon carbide) (Gupta, 2010). The results from the Poole-Frenkel conduction plot ((ln(J/E) vs $E^{1/2}$) showed that a fixed electric field range enables the Poole-Frenkel conduction to maintain its validation and proven useful for the oxide films of 4H-SiC characterization (Gupta, 2010). Another research on silicon carbide was the experiment for Poole-Frenkel emission on individual silicon carbide nanowires through the means of field emission transport measurements (Choueib, 2011). The results showed that the Poole-Frenkel model gives an outstanding fit after using various transport mechanism measurements on the silicon carbide nanowires (Choueib, 2011). This also showed how a field emission can be used as a means of transport measurements on individual semiconducting nanowires (Choueib, 2011).

It is long known that metal/Tin-Dioxide/metal sandwich configuration in metal oxide semiconductor enables a Poole-Frenkel effect to occur where a potential field-assisted lowering of the barrier between conduction band edge and donor-like center (Chenari, 2011). Therefore, the study of these configurations helps to understand the impact of Poole-Frenkel emission. In this research, a Cu/nano-$SnO_2$/Cu sandwich configuration was studied by current-voltage measurements at room temperatures (Chenari, 2011). The results indicated that a noticeable characteristic clearly appearing in the characterization of current-voltage characteristics which are the Poole-Frenkel emission and space charge-limited conduction mechanisms (Chenari, 2011).

Meanwhile, in a metal/insulator/oxide semiconductor configuration comprised of two terminals, it is important to understand the electrical change transport mechanism through an insulator in order to create a better device for advanced electronic applications such as next-generation memories of resistance differences. A study was selected and studied on $Al_2O_3$ insulator in $P^{++}$-Si anode/$Al_2O_3$/IGZO cathode configuration (Lee, 2019). The results observed from the current-voltage characteristics of the diodes showed that the charge carrier transport mechanism changes depending on the differences of defect/leakage density, oxygen vacancy level of the $Al_2O_3$, and conduction band minimum of the semiconductor (Lee, 2019). The researchers also determined that Poole-Frenkel emission occurs with a conduction band offset of 1.5 eV but after that, space charge-limited conduction mechanism becomes the dominant conduction mechanism as a larger electric field increased near the cathode (Lee, 2019).

In conclusion, researchers conducted on Poole-Frenkel emission studies were to understand the relationship of charge conduction mechanism associate with high temperature that occurs within the bulk of the material. Poole-Frenkel emission was used to help and enable other researchers to understand the significance of the phenomenon that often occurs when high dielectric constant materials are exposed to high-temperature application and this enables researchers and manufacturers to improve the materials that are vital in the metal oxide semiconductor configuration.

# CHAPTER 3: METHODOLOGY

## 3.1 Introduction

The methodology for this research is divided into three parts which are the flow chart, synthesis (can be seen in figure 3.2), and self-assembly of the functionalized $Fe_3O_4$-$\gamma$-$Fe_2O_3$ nanoparticles (FNPs) on $SiO_2$/n-Si structure. The flow charts shown in Figure 3.1 are the steps that are needed to satisfy the research objectives. The process and method of synthesis and self-assembly of $Fe_3O_4$-$\gamma$-$Fe_2O_3$ nanoparticles come from the research conducted by A. A. Baharuddin (2017). The research objectives are to investigate the Schottky and Poole-Frenkel emission mechanisms in $Fe_3O_4$-$\gamma$-$Fe_2O_3$ (maghemite magnetite) in the $SiO_2$/n-Si system. Furthermore, the computation and comparisons of the dynamic dielectric constants, $k_r$ in the oxynitride material will be checked through Schottky and Poole-Frenkel emission mechanisms in the maghemite-magnetite nanoparticle.

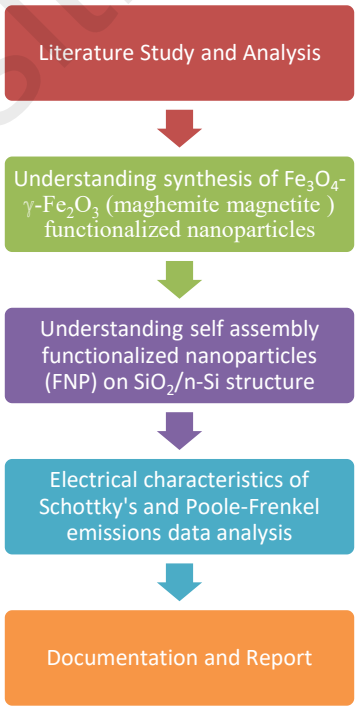


Figure 3.1: Flow Chart of Methodology in Research Project

## 3.2 Synthesis

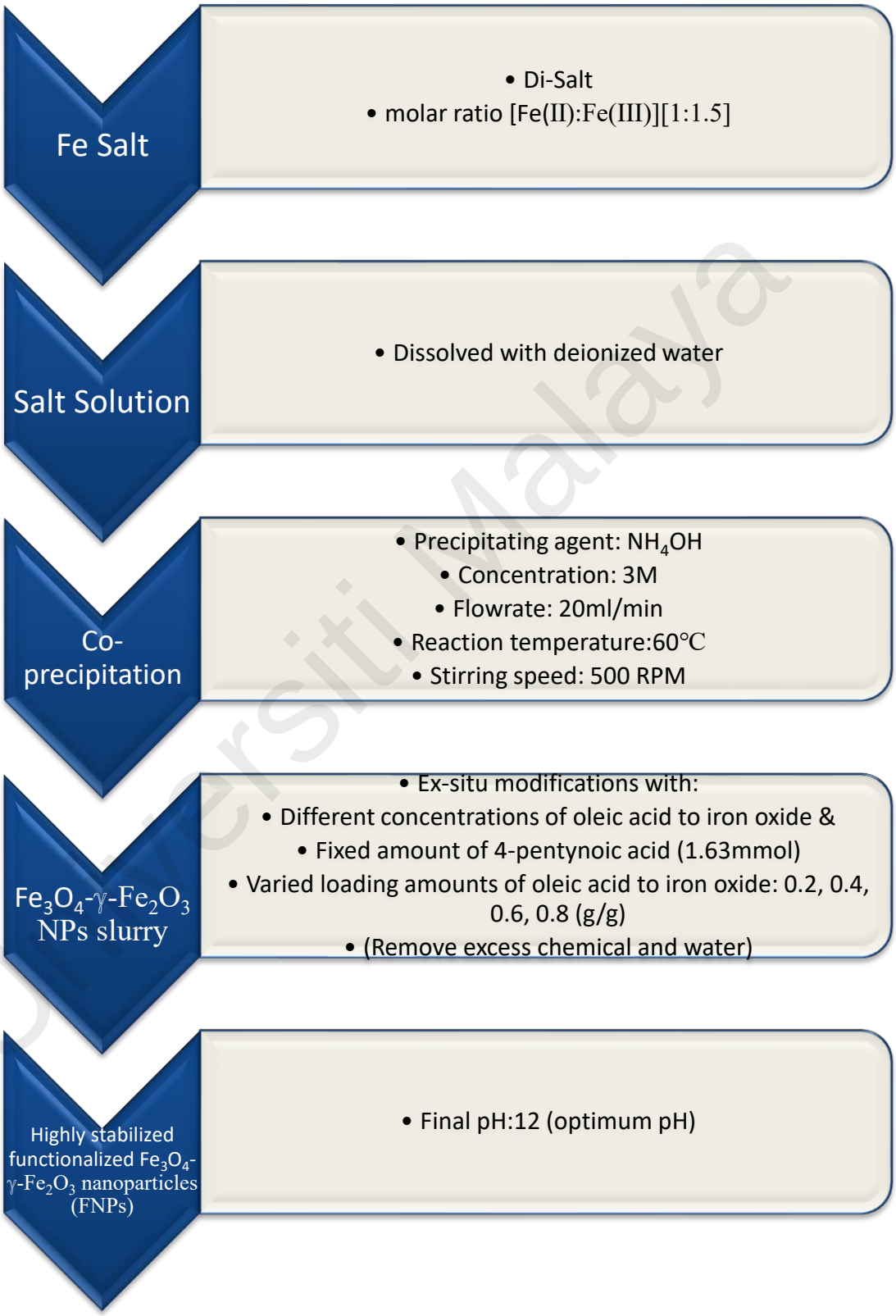


Figure 3.2: Synthesis of $Fe_3O_4$-γ-$Fe_2O_3$ nanoparticles (FNPs)

### 3.2.1 Materials

The chemicals used were of analytical grade in which purity > 99% and without undergoing purification process. The material purchased from Merck were Iron (II) chloride tetrahydrate ($FeCl_2.H_2O$), Iron (III) chloride hexahydrate ($FeCl_3.6H_2O$), and ammonium hydroxide ($NH_4OH$) (28%). Meanwhile, the material purchased from Sigma-Aldrich were oleic acid, 4-pentynoic acid, hexane (99%), and ethanol (90%). The solvent used for rinsing purposes was deionized water.

### 3.2.2 Synthesis of Bare Nanoparticles (NPs)

At the beginning of the process, iron oxides that were bare and functionalized had been synthesized. Next, the beaker was filled with 50 ml deionized water which was heated to 60°C. Subsequently, a molar ratio of 1:1.5 of $FeCl_2.4H_2O$ and $FeCl_3 \cdot 6H_2O$ were mixed into the beaker. The speed of 500 rpm was used to mechanically stir the mixture. 350ml of 3M $NH_4OH$ was gradually added at 20ml/min into the mixture using a burette in which was stirred constantly at 500 rpm at 60°C. The color of the precipitation was progressively turned to black from the initial brown during the process. Magnetic iron oxide was presumed to be the black precipitation.

The mixture was stirred at the speed of 500 rpm at 60℃ for about an hour as the remaining $NH_4OH$ was poured into the beaker. Then, the mixture was placed in the still position to allow magnetic oxide in the beaker to subside to the bottom of the beaker. The precipitate that was leftover was rinsed with 2L of deionized water after the $NH_4OH$ mixture was decanted. The beaker will then be placed on top of the commercial magnets that were compiled together on a base. This procedure was done to allow the precipitate to subside at the bottom of the beaker due to the magnetic attraction of the magnet and the black magnetic precipitate while the excess water was being decanted. The bare iron oxide NPs were labeled as IO samples which were used as a control. The NPs oxidation rate was minimized by storing the sample in a semi-fluid mixture at 4℃.

### 3.2.3 Synthesis of Functionalized Nanoparticles (FNPs)

First and foremost, the process of altering the bare IO NPs to pH 12 was done by pouring in a proportioned amount of $NH_4OH$. Next, a concentration of 0.2, 0.4, 0.6, and 0.8 g/g oleic acid were added to iron oxide in proportion to the 15g total solid content of the bare iron oxide semi-fluid mixture. A glass rod was used to stir the mixture to ensure equal coverage of oleic acid onto the surface of the iron oxide NPs. Then, the excess water was drained from the semi-fluid mixture after the addition of the iron oxide NPs. After that, any excess oleic acid was removed by rinsing the iron oxide with ethanol in addition to hexane. The ex-situ coated oleic acid of the sample labeled as 0.8 that will be used as another control to compare with a sample of concentration of ex-situ oleic acid-coated iron oxide NPs with functionalized 4-pentynoic acid. The concentration of the former was selected due to the preliminary test underline the zeta potential of 0.8 g/g oleic acid to iron oxide were at greater stability hydrodynamic stability (-62.01 ± 0.03 mV) in comparison to the rest of the concentrations. The chances of a successful functionalization of surfactants will be affected by the greater hydrodynamic stability (Jiang, 2014).

In addition, a mixture of iron oxide semi-fluid will be mixed with each of 5g total solid content of 0.2, 0.4, 0.6, and 0.8 g/g oleic acid into 4 different beakers respectively. Then, a fixed amount of 1.63 mmol 4-pentynoic acids were added to each beaker. Next, a complete functionalization of the 4-pentynoic acid with the iron oxide FNPs was ensured by heating the mixture at 60°C under nitrogen gas, $N_2$ while continuously stirred for about 10 hours. The presence of terminal alkyne in 4-pentynoic acid which would bond with $SiO_2$ and forming linkages with the NPs was the main reason why 4-pentynoic acid was chosen. The instigator to the self-assembly that was predicted between the FNPs and the $SiO_2$ was the terminal alkyne. The final products of the ex-situ oleic acid-coated iron oxide NPs that functionalized with 4-pentynoic acid were P-0.2, P-0.4, P-0.6, and P-0.8 labeled samples. Before storing the samples at 4°C in semi-fluid form, the samples were allowed to be cooled. Self- assembly, and characterizations required the samples to be in a condition of pH 12.

### 3.3 Self-assembly

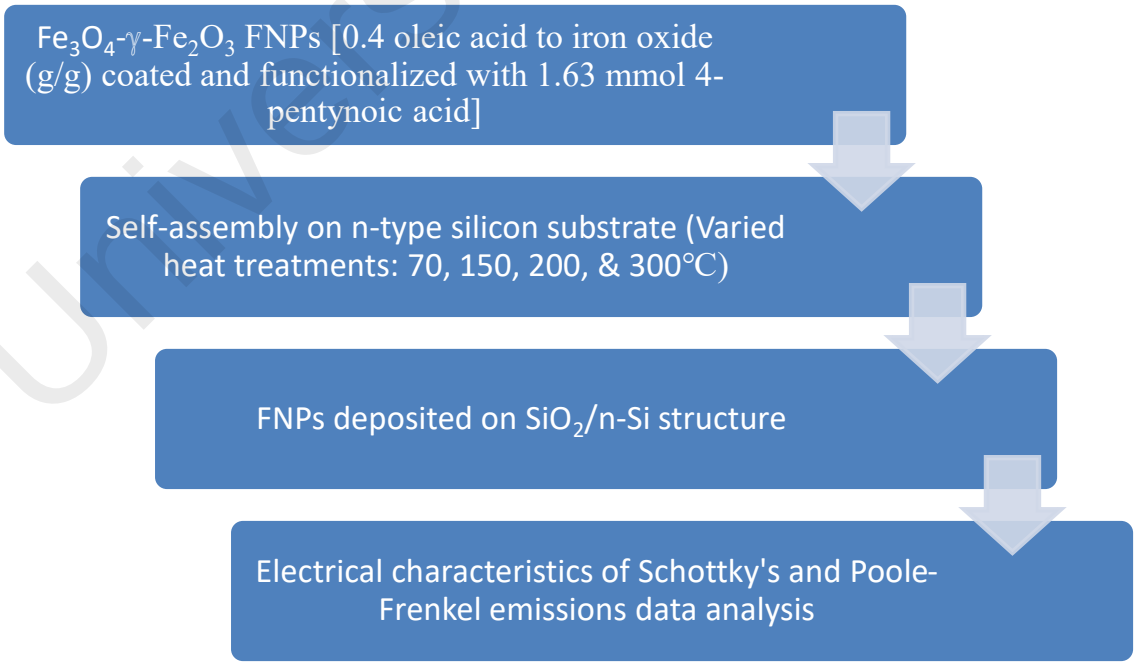


Figure 3.3: Self-Assembly of $Fe_3O_4$-γ-$Fe_2O_3$ NP (FNPs) on Silicon Dioxide

### 3.3.1 Self-assembly of FNPs on $SiO_2$/n-Si structure

Self-assembly of the functionalized $Fe_3O_4$-$\gamma$-$Fe_2O_3$ FNPs was performed in the second part of the process. The thermal oxidation process was used to applied heat treatment in the self-assembly through the grown $SiO_2$ on the surface of the Si substrate. Then, the self-assembly process of the FNPs was done on the surface of the $SiO_2$.

First and foremost, by using Standard Radio Corporation America (RCA) cleaning procedures, the 1 x 1 $cm^2$, n-type, (100)-oriented, 1-10 Ω Si substrates were cleaned. Subsequently, via a micropipette (2-20 µL, Eppendorf), 3µL of the functionalized NPs were drip on the surface of the substrates. Heating was applied to the sample using Carbolite Tube Furnace (CTF) in 10℃/min heating rate and argon gas of 150mL/min flow rate with a range of temperatures from 70℃, 150℃, 200℃, and 300℃ about 60 min. The temperature range of heating was done with the purpose to examine the effect on the surface of the substrate in addition to the morphological and electrical characteristics of the FNPs film.

## 3.4 Electrical Characterizations Schottky and Poole-Frenkel Emission Analysis

The data of J-E (current density vs. current field) was developed from I-V (current-voltage) measurements that were acquired from a computer-controlled SPA system. A. A. Baharuddin (2017) had conducted an experiment to determine one of the electrical characterizations of the $Fe_3O_4$-$\gamma$-$Fe_2O_3$ functionalized nanoparticles on $SiO_2$/n-Si structure which was the Fowler-Nordheim tunneling effect. The next electrical characterization for this research will be using Schottky and Poole-Frenkel emission theorem with the J-E data retrieved from previous A. A. Baharuddin (2017) research. The results of the electrical characterization research will be retrieved by using the following equations for standard Schottky emission and Poole-Frenkel emission.

# CHAPTER 4: RESULTS AND DISCUSSION

## 4.1 Ohm's Law and Trap-Filled Limit (TFL) Limiting Mechanisms

One of the aims of this research project is to investigate and study the Schottky and Poole-Frenkel emission mechanism in $Fe_3O_4$-gamma-$Fe_2O_3/SiO_2$/n-type silicon system. This was done by analyzing obtained data from the current density vs. the current field (J-E) characteristic graph that was previously conducted from the research of A. A. Baharuddin (2017). Figure 4.1 shows the obtained data of current density vs. the current field (J-E) characteristic graph of $Fe_3O_4$-gamma-$Fe_2O_3/SiO_2$. The J-E graph in figure 4.1 also showed that there is one instantaneous increment of leakage current density that occurred during the experiment. This instantaneous increment is also be known as soft breakdown ($E_B$) (Wong, 2011).

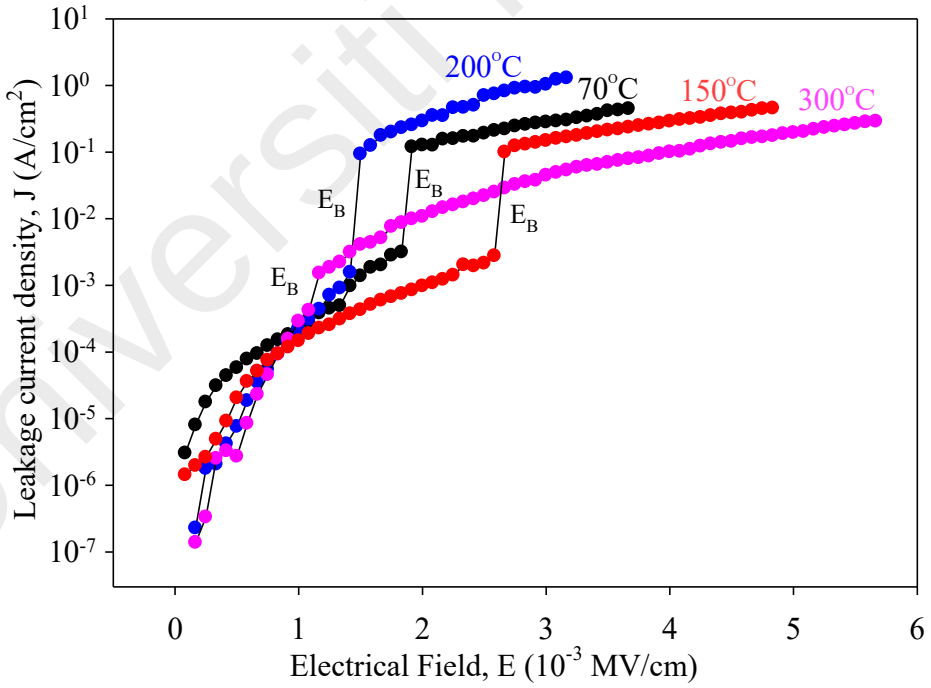


Figure 4.1: J-E Characteristics of $Fe_3O_4$-gamma-$Fe_2O_3/SiO_2$ Prepared Films (A. A. Baharuddin, 2017)

Even though the main objective of this research project is to investigate Schottky and Poole-Frenkel emission as well as to identify the dynamic dielectric constant of both type of emissions; there is no doubt that there are several possible charge conduction mechanisms that could occur and are responsible for the leakage current in $Fe_3O_4$-gamma-$Fe_2O_3$/$SiO_2$/n-type silicon system. One of the mechanisms involved in the current leakage is the Space-Charge-Limited conduction (SCLC) mechanism. This working of this mechanism is akin to electrons transport conduction in a vacuum diode (F-C. Chiu, 2014).

SCLC mechanism occurs when electrons are impelled into the oxide of ultralow gate voltage before the electrons entered through the oxide at high gate voltage (Wong, 2011). This phenomenon started as the density of the accumulated electrons at the majority carriers in n-type Si are much denser than the density of free carriers available which enable the electrons to penetrate into the oxide (Wong, 2011). Lampert (1956) mentioned that through defect and impurity of the insulators are sufficient enough to induce low-density free carriers and inevitably charge unbalance can be simply produced by the electric fields. The penetration of the electrons into the oxide enable a space charge region to be formed which will block or reduce the electrons from penetrating into the oxide (Wong, 2011). This means that the SCLC mechanism occurs before the Schottky and Poole-Frenkel emission takes place as the Schottky and Poole-Frenkel emission occurs at higher gate voltage.

In order to identify the SCLC mechanism as stated by Lampert's theory, the current density-voltage characteristic is used and constricted by three limiting mechanisms which are Ohm's law, Trap-Filled-Limit (TFL) conduction, and Child's law (Lampert, 1956). However, it is sufficient for using only Ohm's law and TFL conductions to analyze and determine the SCLC mechanism in this research project. This is due to the necessary information of the approximation number of traps in the investigated sample cannot be obtained due to unavailable information of the approximation used for the Child's law conduction mechanism.

The mechanisms of Ohm's law and Trap-Filled-Limit (TFL) conduction can be mathematically described as follow (Wong, 2011):

$$J_{Ohm} = qn_o \mu V_g / t_{ox} \tag{4.1}$$

$$J_{TFL} = B\left(V_g{}^{l+1} / t_{ox}{}^{2l+1}\right) \tag{4.2}$$

Where $V_g$ is the surface potential of Si at a specific gate voltage, $t_{ox}$ is the thickness of the oxide or interfacial layer which is 12.6 μm (A. A. Baharuddin, Ang, B.C., Wong, Y.H., 2017), $n_o$ is the thermal equilibrium of the concentrated free charge carriers, B is an *l*-dependent parameter where *l* also denoted as:

$$l = T_c / T \tag{4.3}$$

$T_c$ stands for the characteristic temperature of trap distribution while T is the absolute temperature. The rest of the symbols have already been described earlier in Schottky emission model equations. The equation of 4.1 and 4.3 are used to construct figure 4.2 graph of a family of J-$V_g$ measured at various temperatures and fitted with Ohm's law (J α $V_g$) and TFL conduction (J α $V_g{}^n$ where n is denoted as n = *l*+1).

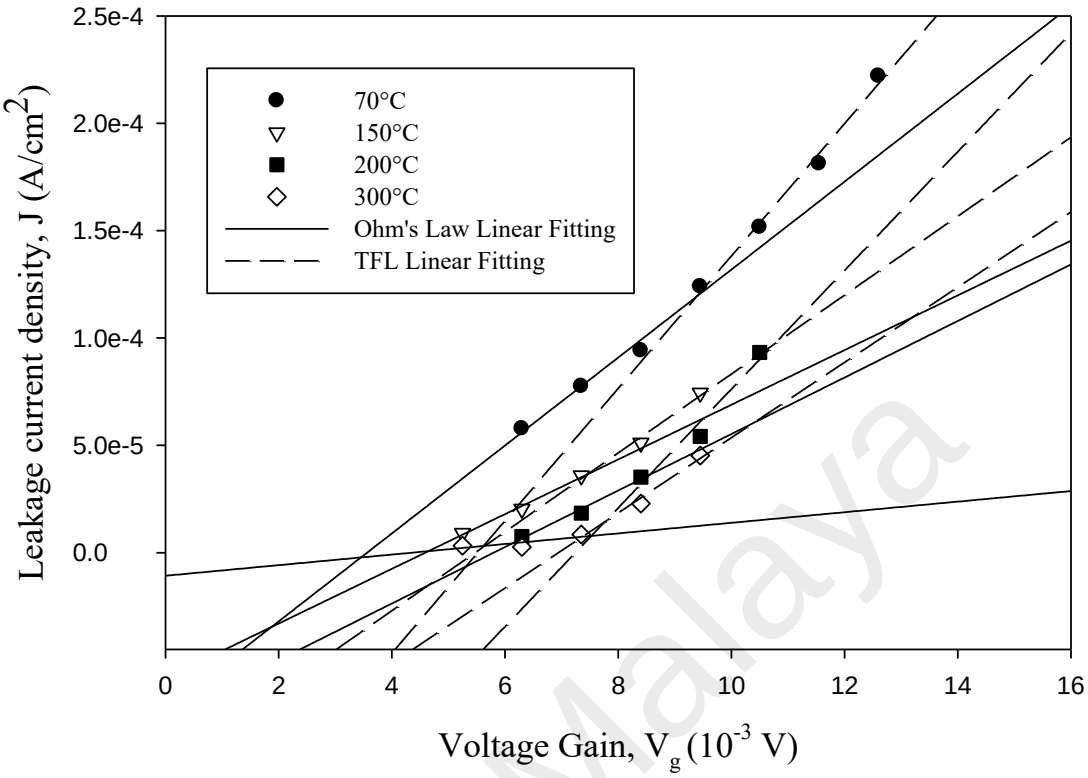


Figure 4.2: Ohm's Law and Trap-Filled-Limit (TFL) Conduction Plot

The sigmoid curve of the graph in figure 4.2 showed that Ohm's law linear fitting occurs before the Trap-Filled-Limit (TFL) conduction mechanism. This can be seen as the electric field increases; the oxides undergo the TFL conduction process which suggested that Ohm's law limiting mechanism is the first trigger in the Space-Limited-Charge Conduction (SCLC) mechanism and followed by the TFL conduction process. The gradients of Ohm's law and TFL were obtained from the linear fitting/extrapolation and shown in figure 4.3 and 4.4 respectively.

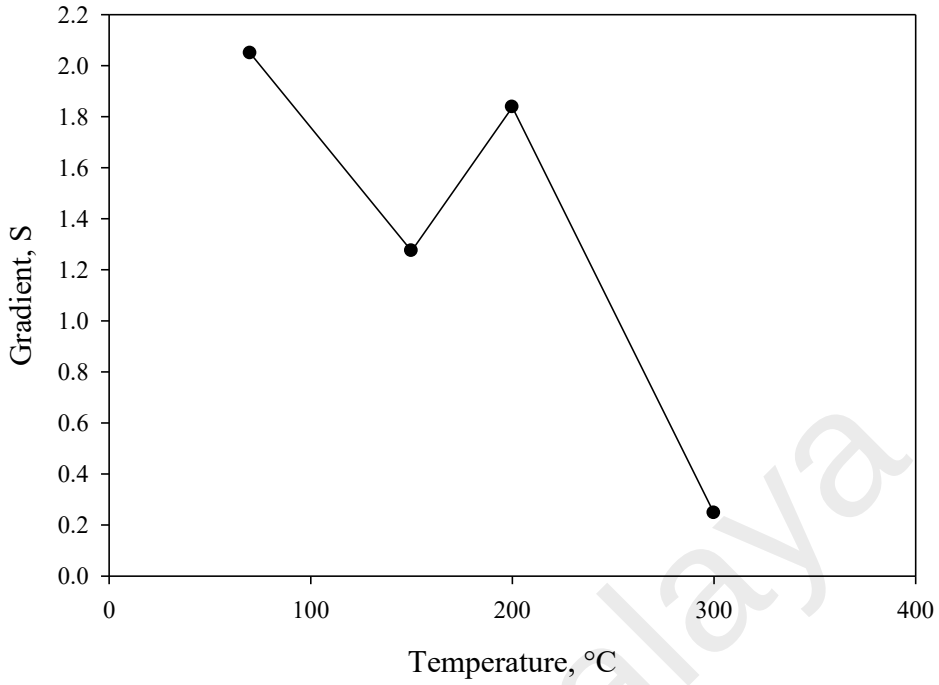


Figure 4.3: Gradient of J-$V_g$ Plot Fitted with Ohm's Law

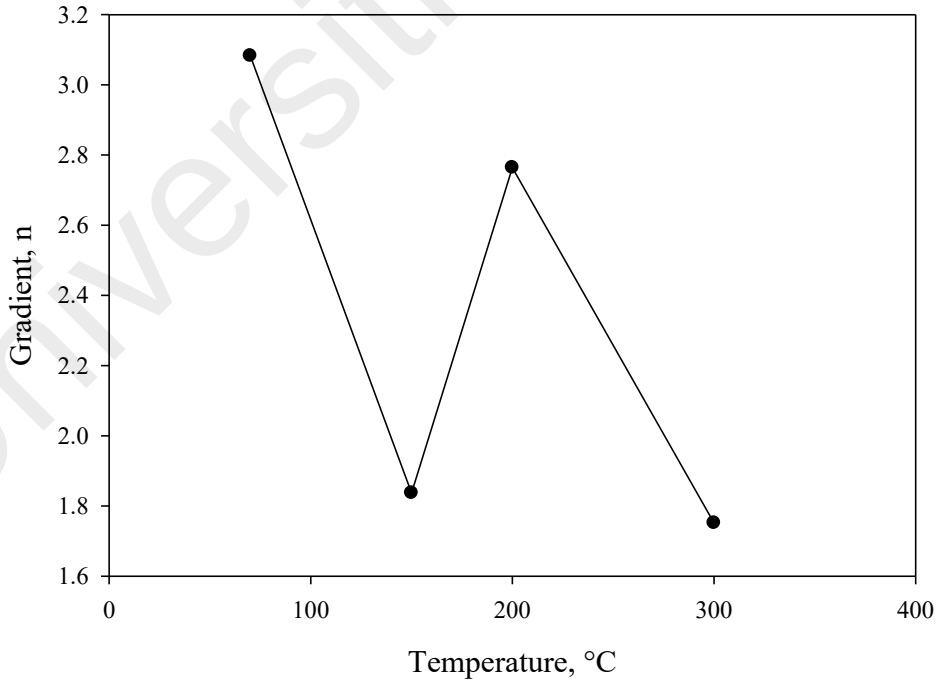


Figure 4.4: Gradient of J-$V_g$ Plot Fitted with TFL Conduction

In order for charge conduction to follow Ohm's law, the gradient of the slope (S) preferably should be 1 (Lampert, 1956). The extracted gradients from the data in figure 4.2 were analyzed and compared to 1 and presented as a function of temperature in figure 4.3. However, only 150°C temperature achieved to near 1 value while the rest are higher or lower than 1. Therefore, it is sufficient to say that the gradients of the graph do not follow Ohm's law. After that, the oxides would encounter a TFL conduction process as the electric field increases as shown in figure 4.4. The gradient of the TFL conduction from the linear fitting/extrapolation in figure 4.2 were plotted in the graph in figure 4.4. The results from figure 4.4 showed that the gradients vary as the temperature increased where after 200 °C, the n value dropped rapidly. This indicates that the reduction of n value after 200 °C was caused by the lowering of the density of the oxide and oxide-semiconductor traps.

The results of Ohm's law and TFL conduction showed that a portion of the SCLC mechanism does occur during low electric field but does not contribute to the soft breakdown experienced by the material. This can be seen early on when comparing figure 4.1 and figure 4.2 where the SCLC mechanism does not directly contribute to soft breakdown. However, the results from the analysis showed that there is a possibility of other types of conduction mechanisms that could occur while conducting the experiment from low electric to a high electric field.

## 4.2 Schottky Emission Mechanism

Schottky and Poole-Frenkel emission mechanism graph can then be generated by using the data obtained from figure 4.1. The J-E characteristic data are rearranged and recalculated using the standard Schottky and Poole-Frenkel emission models. The standard Schottky emission model can be expressed as (Wong, 2011):

$$J_{SE} = A^{*}T\ exp\frac{\{-q[\Phi_B - (\frac{qE}{4\pi k_r \varepsilon_o})^{\frac{1}{2}}}{kT} \quad (4.4)$$

Where A* is termed as effective Richardson constant is shown which is the unit of $A/cm^2k^2$ below,

$$A^{*} = \left(\frac{4\pi q m^{*} k^2}{h^3}\right) = 120\left(\frac{m^{*}}{m_o}\right) \quad (4.5)$$

$J_{SE}$ is the current density governed by Schottky emission, T is the measured temperature, q is the electric charge, $\Phi_B$ is the Schottky barrier height, E is the electric field across the dielectric, $k_r$ is the dynamic dielectric constant of the oxide, $\varepsilon_o$ is the permittivity of the vacuum, k is the Boltzmann's constant, h is the Planck constant, and $m^*$ is the effective electron mass in the oxide, where $m^*= 0.3m_o$, in which $m_o$ is the free electron mass in the oxide, where $m^*= 0.3m_o$, in which $m_o$ is the free electron mass. The graph in figure 4.5 shown a Schottky emission mechanism graph of a family of $ln(J/T^2)$ vs $E^{1/2}$ plot with various temperatures (70-300°C).

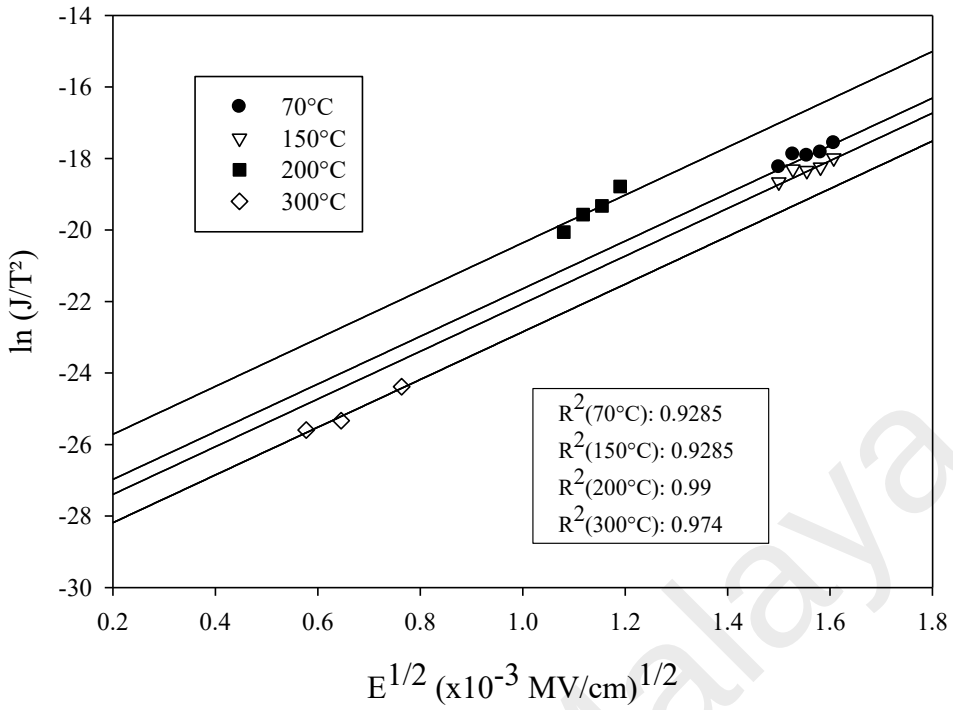


Figure 4.5: Schottky Emission Plot

The sigmoid curves of the graph in figure 4.5 indicate the fitting of the Schottky emission mechanism. The obtained $R^2$ values were ranged from 0.929-0.99 and were derived from linear fitting/extrapolation of the Schottky emission graph. This showed that the data plotted are well-fitted with the standard Schottky emission model. In the usual standard Schottky emission, the plotted graph of $\ln(J/T^2)$ vs. $E^{1/2}$ should be linear (F-C. Chiu, 2006; Wong, 2010). The data from figure 4.5 then was used to identify the dynamic dielectric constant and barrier height of Schottky emission.

The Schottky emission model from equation 4.4 is rearranged for the analysis of figure 4.5 graph where the analysis of Schottky emission mechanism's equation will become (Botzakaki, 2020):

$$\ln J/T^2 = \ln A^* - q\Phi_B/kT + \left(\sqrt{q^3E/4\pi k_r\varepsilon_0}/kT\right) \quad (4.6)$$

The equation 4.6 and the data in figure 4.5 are utilized to determine the gradient of the fitted lines which provide the detailed dynamic dielectric constant, $k_r$ graph of Schottky emission that can be seen in figure 4.6.

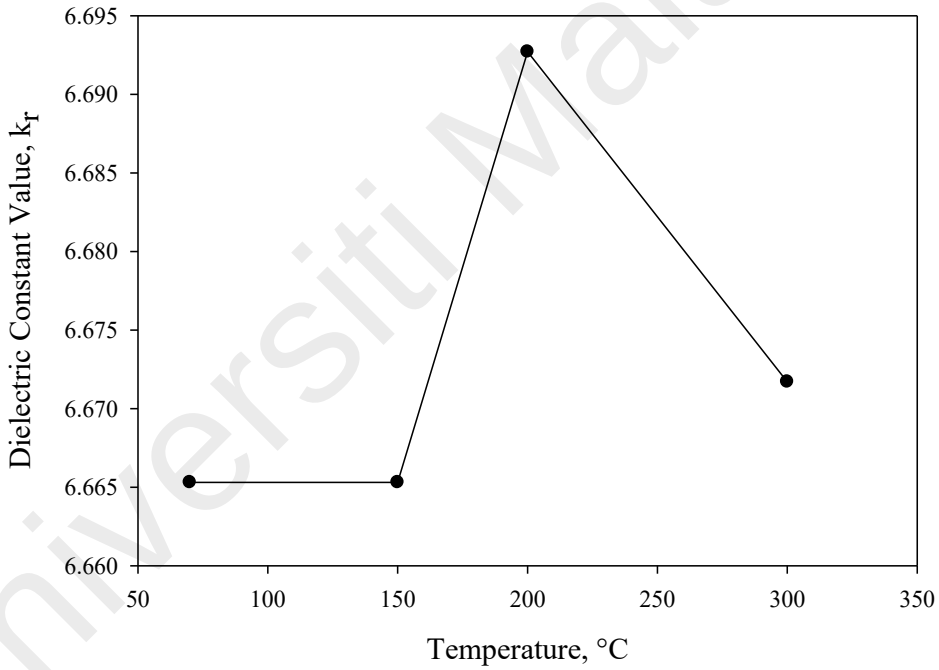


Figure 4.6: Dynamic Dielectric Constant, $k_r$ of Schottky Emission Graph

Figure 4.6 shows the highest value of dynamic dielectric constant, $k_r$ which is 6.6927 at 200°C. One of the methods to compare the dynamic dielectric constant value is to use the refractive index of the material as a comparison. However, there is no definite value of the refractive index that was observed or obtained from other sources for magnetite-maghemite iron oxide nanoparticles to this date. Therefore, the refractive index value of magnetite (iron (II, III) oxide) will be used as the main comparison to compare with the dielectric constant of the experiment. The refractive index of magnetite ($Fe_3O_4$) is around 6.76 where the refractive index square value, $n = k_r^{1/2} = 2.6$ (W. Kim, Suh, C-Y., Cho, S-W., Roh, K-M., Kwon, H., Song, K. Shon, I-J. , 2012). The range of the fitted $k_r$ values of 6.6653-6.6927 are well matched to the refractive index of magnetite obtained from (W. Kim, Suh, C-Y., Cho, S-W., Roh, K-M., Kwon, H., Song, K. Shon, I-J. , 2012). The graph in figure 4.6 showed that the dynamic dielectric constant value peak at the optimum temperature at 200°C and decreasing at 300°C.

The next step is to use the derivation from equation 4.6, the intercept of the fitted lines of figure 4.5 are then to be used in deriving and calculating the barrier height of Schottky emission, $\Phi_B$ where (Botzakaki, 2020):

$$C = \ln A^* - q\Phi_B/kT \tag{4.7}$$

The results of the barrier height calculations can be seen from the graph of Schottky emission barrier height against temperature in figure 4.7.

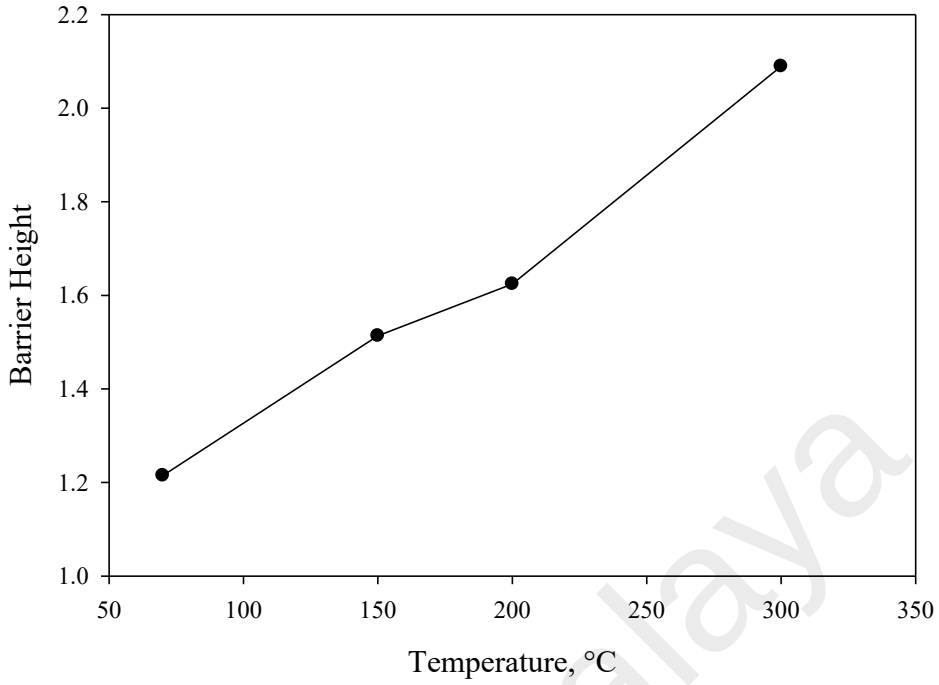


Figure 4.7: Barrier Height, $\Phi_B$ of Schottky Emission Graph

The highest barrier height, $\Phi_B$ that be obtained from figure 4.7 is 2.084 at 300°C. The barrier height from the graph shows that as the temperature increased, so does the barrier height of the magnetite-maghemite silicon oxide material. However, the decreasing dielectric constant value of the material at the temperature of 300°C that can be seen in figure 4.7 would ultimately help the electron charges to overcome the high barrier height. Hence, the results from the analysis showed that the magnetite-maghemite nanoparticle synthesized on the silicon oxide capable to withstand high temperature of the condition up to 200°C where the barrier height is at 1.6242.

## 4.3 Poole-Frenkel Emission Mechanism

Meanwhile, by using J-E characteristic data from figure 4.1, a similar fitting procedure was used in generating the Poole-Frenkel emission mechanism graph using the Poole-Frenkel emission model. This is due to Poole-Frenkel emission is a thermionic emission of electrons from the bulk of the oxide which is similar to Schottky emission (Wong, 2011). The standard Poole-Frenkel emission model can be expressed as (Wong, 2011):

$$J_{PF} = (qN_c\mu)E \ \exp\{-q[\Phi_t-(qE/\pi k_r\varepsilon_o)^{1/2}]\}/kT \qquad (4.8)$$

Where $J_{PF}$ is termed as the current density of Poole-Frenkel emission, $\mu$ is the electronic mobility in oxide, $N_c$ is the state density of the conduction band and $\Phi_t$ is the state density of the trap energy level in the oxide. The rest of the symbols have been described earlier in Schottky emission model equations. Figure 4.8 shows a Poole-Frenkel emission mechanism graph of a family of ln(J/E) vs $E^{1/2}$ plot with various temperatures (70-300°C).

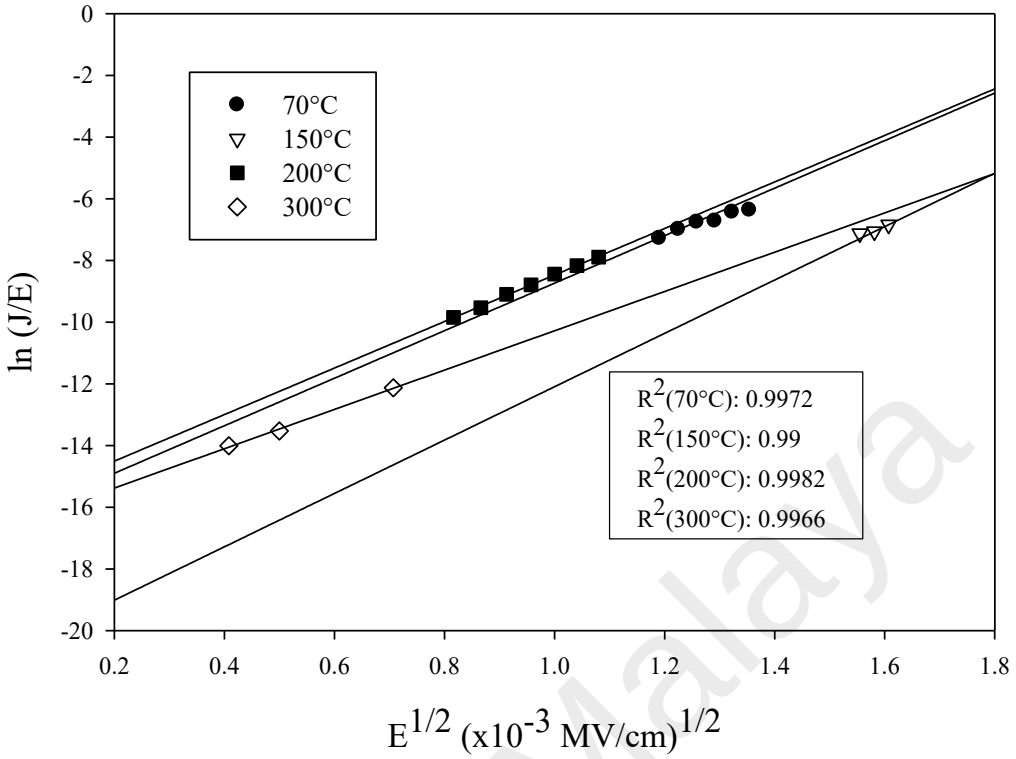


Figure 4.8: Poole-Frenkel Emission Plot

The sigmoid curves of the graph in figure 4.8 indicate the fitting of the Poole-Frenkel emission mechanism. The obtained $R^2$ values were ranged from 0.99-0.9982 and were derived from linear fitting/extrapolation of the Poole-Frenkel emission graph. The $R^2$ values in figure 4.8 indicate that the data are well-fitted with the standard Poole-Frenkel emission model (Equation 4.8).

The Poole-Frenkel emission model from equation 4.8 is then can be rearranged for the analysis of figure 4.8 graph where the analysis of Poole-Frenkel emission mechanism's equation will become (Botzakaki, 2020):

$$\ln J/E = \ln(qN_c\mu) - q\Phi_t/kT + \left(\sqrt{q^3E/4\pi k_r\varepsilon_0}/kT\right)\sqrt{E} \qquad (4.9)$$

The equation 4.9 and the data in figure 4.8 are used to determine the gradient of the fitted lines which provide the detailed dynamic dielectric constant, $k_r$ graph of the Poole-Frenkel emission that can be seen in figure 4.9.

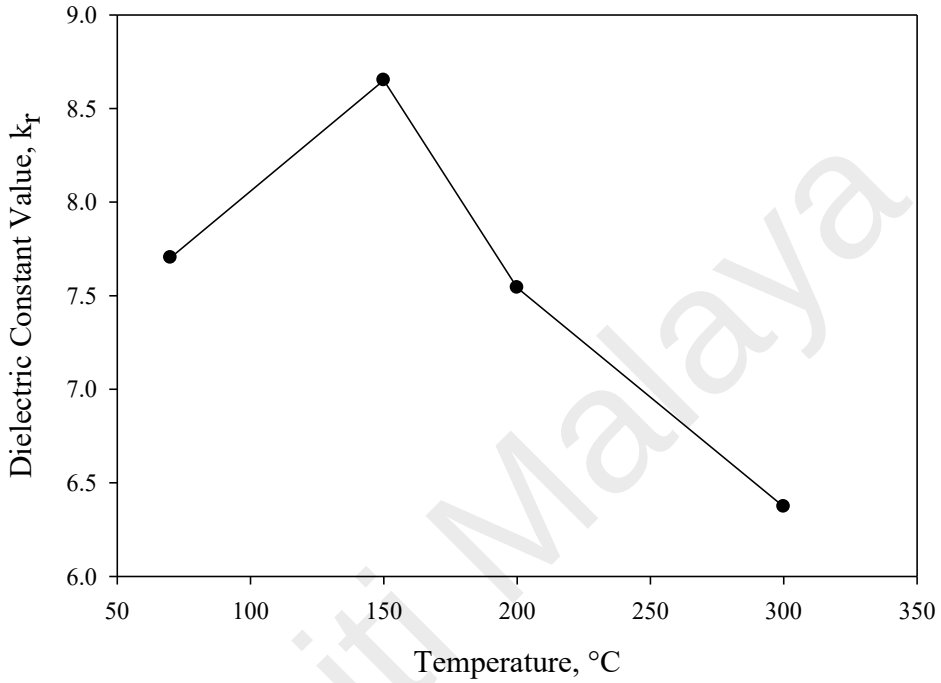


Figure 4.9: Dynamic Dielectric Constant, $k_r$ of Poole-Frenkel Emission Graph

The highest value of the dynamic dielectric constant value, $k_r$ obtained from figure 4.6 is 8.6505 at 150°C. The fitted dynamic dielectric constant, $k_r$ values are in the range of 6.3721-8.6505 which showed that there are well-matched with the refractive index of magnetite ($Fe_3O_4$) (W. Kim, Suh, C-Y., Cho, S-W., Roh, K-M., Kwon, H., Song, K. Shon, I-J. , 2012). The graph also showed that the optimum dielectric constant value is at 150°C and after that, the dielectric constant value decreased as the temperature increased. This indicates that the dynamic dielectric constant is the highest at 150°C and after that, the current leakage due to Poole-Frenkel emission occurs where the dynamic dielectric constant is reduced as the temperature increased.

# CHAPTER 5: CONCLUSIONS

In conclusion, the electrical characterizations of Schottky and Poole-Frenkel emission mechanisms in $Fe_3O_4$-γ-$Fe_2O_3$/$SiO_2$/n-type Si system are investigated through analysis from J-E characteristic data of $Fe_3O_4$-γ-$Fe_2O_3$/$SiO_2$/n-type Si as well as to determine and compare the dynamic dielectric constant, $k_r$ caused by Schottky and Poole-Frenkel emission. The following conclusions that can be gained from the results obtained as follows:

(1) The analysis of Ohm's law and TFL conduction showed that a portion of the SCLC mechanism occurs but does not contribute to the soft breakdown experienced by the $Fe_3O_4$-γ-$Fe_2O_3$/$SiO_2$/n-type Si system.

(2) The sigmoid curve linear fitting of Schottky and Poole-Frenkel emission mechanisms are well fitted with the standard model equations respectively by using the $R^2$ values obtained from the linear fitting graphs.

(3) The highest dynamic dielectric constant, $k_r$ of Schottky emission is 6.6927 at 200°C, while the highest dynamic dielectric constant $k_r$ of Poole-Frenkel emission is 8.6505 at 150°C. Both of the Schottky and Poole-Frenkel dynamic dielectric constants ranged values are well-matched with the refractive index of magnetite ($Fe_3O_4$).

(4) The highest barrier height, $\Phi_B$ of the Schottky emission mechanism is 1.6242 at 200°C. This is due to at 300°C, the dynamic dielectric constant of Schottky emission decreases rapidly and could cause the electrons to overcome the barrier height.

(5) The overall results showed that Schottky and Poole-Frenkel emission mechanism leakage current contributed to the soft breakdown of the material which happened in a high electric field and high-temperature environments.

## REFERENCES


Arns, R. G. (1998). The Other Transistor: Early History of The Metal Oxide Semiconductor Field-Effect Transistor. *Engineering Science and Education Journal, 7*(5), 233-240. doi:10.1049/esej:19980509

Baharuddin, A. A. (2017). *Self-Assembly of Synthesized 4-Pentynoic Acid Functionalized Magnetite-Maghemite Nanoparticles on Silicon Dioxide/N-Type Silicon Substrate.* (Master ), University of Malaya, Kuala Lumpur, Malaysia.

Baharuddin, A. A., Ang, B.C., Wong, Y.H. (2017). Self-Assembly and Electrical Characteristics of 4-pentynoic acid functionalized Fe3O4-γ-Fe2O3 nanoparticles on SiO2/n-Si. *Applied Surface Science, 423*, 236-244. doi:https://doi.org/10.1016/j.apsusc.2017.06.155

Bersch, E. (2008). *Energy Level Alignment in Metal Oxide Semiconductor and Organic Dye Oxide Systems.* (Doctor of Philosophy), Rutgers University. Retrieved from https://rucore.libraries.rutgers.edu/rutgers-lib/24481/

Botzakaki, M. A., Skoulatakis, G., Papageorgiou, G.P., Krontiras, C.A. (2020). Interfacial Characterization and Transport Conduction Mechanisms in Al/HfO2/p-Ge Structures: Energy Band Diagram. *Semiconductor Structures, Low Dimensional Sustems and Quantum Phenomena, 54*(5), 543-553. doi:10.1134/S1063782620050036

Britannica, T. E. o. E. (2016). Schottky Effect. Retrieved from https://www.britannica.com/science/Schottky-effect

Chen, K.-H., Tsai, T-M., Cheng, C-M., Huang, S-J., Chang, C-K., Liang, S-P., Young, T-F. . (2018). Schottky Emission Distance and Barrier Height Properties of Bipolar Switching Gd:SiOx RRAM Devices under Different Oxygen Concentration Environments. *Materials (Basel), 11 (1)*(43), 1-7. doi:10.3390/ma11010043

Chenari, H. M., Sedghi, H., Talebian, M., Golzan, M.M., Hassanzadeh, A. . (2011). Poole-Frenkel Conduction in Cu/Nano-SnO2/Cu Arrangement. *Journal of Nanomaterials, 2011*, 1-4. doi:https://doi.org/10.1155/2011/190391

Cheong, K. Y., Moon, J.H., Kim, H.J., Bahng, W., Kim, N-K. (2008). Current Conduction Mechanisms in Atomic-Layer-Deposited HfO2/nitrided SiO2 stacked gate on 4H Silicon Carbide. *Journal of Applied Physics, 24*(27), 5371-5378. doi:https://doi.org/10.1142/S0217979210055925

Chiu, F.-C. (2006). Interface Characterization and Carrier Transportation in Metal/HfO2/Silicon Structure. *Journal of Applied Physics, 100*(11), 4102-4101-4102-4105. doi:https://doi.org/10.1063/1.2401657

Chiu, F.-C. (2007). Electrical Characterization and Current Transportation in Metal/Dy2O3/Si Structure. *Journal of Applied Physics, 102*(4), 4116-4111-4116-4115. doi:https://doi.org/10.1063/1.2767380

Chiu, F.-C. (2014). A Review on Conduction Mechanisms in Dielectric Films. *Thin Film Applications in Advanced Materials, 2014*, 1-19. doi:https://doi.org/10.1155/2014/578168

Chiu, F.-C., Lee, C-Y., Pan, T-M. . (2009). Current Conduction Mechanisms in Pr2O3/Oxynitride Laminated Gate Dielectrics. *Journal of Applied Physics, 105*(7), 4103-4101-41034. doi:https://doi.org/10.1063/1.3103282

Chiu, F.-C., Lin, Z-H., Chang, C-W., Wang, C-C., Chuang, K-F., Huang, C-Y., Lee, J. Y-M., Hwang, H-L. (2005). Electron Conduction Mechanism and Band Diagram of Sputter-Deposited Al/ZrO2/Si Structure. *Journal of Applied Physics, 97*(3), 034506-034501-034506-034504. doi:https://doi.org/10.1063/1.1846131

Chiu, F.-C. L., C-M. . (2010). Optical and Electrical Characterizations of Cerium Oxide Thin Films. *Journal of Physics D: Applied Physics, 43*(7), 1-5. doi:10.1088/0022-3727/43/7/075104

Choueib, M., Ayari, A., Vincent, P., Perisanu, S., Purcell, S.T. (2011). Evidence for Poole-Frenkel Conduction in Individual SiC Nanowires by Field Emission Transport Measurements. *Journal of Applied Physics, 109*(7), 3709-3701-3709-3705. doi:https://doi.org/10.1063/1.3556736

Chowdhury, S. R., Yanful, E.K. (2010). Arsenic and Chromium Removal by Mixed Magnetite-Maghemite Nanoparticles and the Effect of Phosphate on Removal. *Journal of Enviromental Management, 91*(11), 2238-2247. doi:https://doi.org/10.1016/j.jenvman.2010.06.003

Chowdhury, S. R., Yanful, E.K. (2013). Kinetics of Cadmium (II) Uptake by Mixed Maghemite-Magnetite Nanoparticles. *Journal of Enviromental Management, 129*, 642-651. doi:https://doi.org/10.1016/j.jenvman.2013.08.028

Chowdhury, S. R., Yanful, E.K., Pratt, A.R. (2012). Chemical States in XPS and Raman Analysis During Removal of Cr (VI) from Contaminated Water by Maghemite-Magnetite Nanoparticles. *Journal of Hazardous Materials, 235-236*, 246-256. doi:https://doi.org/10.1016/j.jhazmat.2012.07.054

Cibert, J., Bobo, J-F., Luders, U. . (2005). Development of New Materials for Spintronics. *Comptes Rendus Physique, 6*(9), 977-996. doi:https://doi.org/10.1016/j.crhy.2005.10.008

Connell, G. A. N., Camphausen, D.L., Paul, W. (1972). Theory of Poole-Frenkel Conduction in Low-Mobility Semiconductors. *The Philosophical Magazine: A Journal of Theoretical Experimental and Applied Physics, 26*(3), 541-551. doi:https://doi.org/10.1080/14786437208230103

De Faria, D. L. A., Silva, S.V., De Oliveira, M.T. . (1997). Raman Micro Spectroscopy of Some Iron Oxides and Oxyhydroxides. *Journal of Raman Spectroscopy, 28*(11), 873-878. doi:https://doi.org/10.1002/(SICI)1097-4555(199711)28:11<873::AID-JRS177>3.0.CO;2-B

Deniz, A. R., Caldiran, Z., Sahin, Y., Sinoforoglu, M., Metin, O., Meral, K., Aydogan, S. (2013). The Synthesis of the Fe3O4 Nanoparticles and the Analysis of the Current-Voltage Measurements on Au/Fe3O4/p-Si Schottky Contacts in a Wide Temperature Range. *Metallurgical and Materials Transactions A, 44 A*, 3809-3814. doi:https://doi.org/10.1007/s11661-013-1716-9

Dhariwal, S. R., Landsberg, P.T. . (1989). A Theoretical Study of Field-Enhanced Emission (Poole-Frenkel Effect). *Journal of Physics and Chemistry of Solids, 50*(4), 363-368. doi:https://doi.org/10.1016/0022-3697(89)90435-6

Electronicshub.Org. (2020). Introduction to MOSFET | Enhancement, Depletion, Amplifier, Applications. Retrieved from https://www.electronicshub.org/mosfet/

Emtage, P. R. a. T., W. (1962). Schottky Emission Through Thin Insulating Films. *Physical Review Letters, 8*(7), 267-268. doi:https://doi.org/10.1103/PhysRevLett.8.267

Eranen, S. (2010). *Chapter 6.1 - Thin Films on Silicon: Silicon Dioxide* (M. Tilli, Motooka, T., Airaksnine, V-M., Franssila, S., Paulasto-Krockel, M. Lindroos, V. Ed.): William Andrew Publishing.

Ghosh, S., Srivastava, P.C. . (2014). Interface States of Fe3O4/Si Interfacial Structure and Effect of Magnetic Field. *Journal of Electronic Materials, 43*(11), 4357-4363. doi:https://doi.org/10.1007/s11664-014-3392-y

Globe, C. (2020). Difference between P-type and N-Type Semiconductor. Retrieved from https://circuitglobe.com/difference-between-p-type-and-n-type-semiconductor.html

Goswami, M. M., Dey, C. Bandyopadhyay, A., Sarkar, D., Ahir, M. (2016). Micelles Driven, Magnetite (Fe3O4) Hollow Spheres and a Study on AC Magnetic Properties for Hyperthermia Application. *Journal of Magnetism and Magnetic Materials, 417*, 376-381. doi:https://doi.org/10.1016/j.jmmm.2016.05.069

Gupta, S. K., Azam, A., Akhtar, J. . (2010). Experimental Analysis of Current Conduction through Thermally Grown SiO2 on Thick Epitaxial 4H-SiC Employing Poole-Frenkel Mechanism. *Pramana-Journal of Physics, 74*(2), 325-330. doi:https://doi.org/10.1007/s12043-010-0030-y

Hosseini-Monfared, H., Pargchegani, F., Alavi, S. (2015). Carboxylic Acid Effects on the Size and Catalytic Activity of Magnetic Nanoparticles. *Journal of Colloid and Interface Science, 437*, 1-9. doi:https://doi.org/10.1016/j.jcis.2014.08.056

Incorporated, M. W. (2020). Metal-Oxide Semi-Conductor. Retrieved from https://www.merriam-webster.com/dictionary/metal-oxide%20semiconductor

Information, N. C. f. B. (2020). PubChem Compound Summary for CID 24261, Silicon dioxide. Retrieved from https://pubchem.ncbi.nlm.nih.gov/compound/Silicon-dioxide

Isai, G. I., Holleman, J., Wallinga, H., Woerlee, P.H. (2004). Conduction and Trapping Mechanisms in SiO2 Films Grown Near Room Temperature by Multipolar Electron Cyclotron Resonance Plasma Enhanced Chemical Vapor Deposition. *Journal of Vacuum Science and Technology B, 22*(3), 1022-1029. doi:https://doi.org/10.1116/1.1736645

Jeong, D. S., Hwang, C.S. . (2005). Tunneling-Assisted Poole-Frenkel Conduction Mechanism in HfO2 thin films. *Journal of Applied Physics, 98*(11), 3701-3701-3701-3706. doi:https://doi.org/10.1063/1.2135895

Jiang, F., Li, X., Zhu, Y., Tang, Z. . (2014). Synthesis and Magnetic Characterizations of Uniform Iron Oxide Nanoparticles. *Physica B: Condensed Matter, 443*, 1-5. doi:https://doi.org/10.1016/j.physb.2014.03.009

Kahng, D., Atall, M.M. (1960). Silicon-Silicon Dioxide Field Induced Surface Devices. *IRE-AIEEE Solid-State Device Research Conference*.

Kim, S., Surek, J., Baker-Jarvis, J., Provenzano, V. . (2012). *Electromagnetic Properties of Iron Oxide Corrosion Product Powders at Radio Frequencies.* Paper presented at the 2012 Conference on Precision Electromagnetic Measurements, Washington DC, USA.

Kim, W., Suh, C-Y., Cho, S-W., Roh, K-M., Kwon, H., Song, K. Shon, I-J. . (2012). A New Method for the Identification and Quantification of Magnetite-Maghemite Mixture using Conventional X-Ray Diffraction Technique. *Talanta, 94*, 348-352. doi:https://doi.org/10.1016/j.talanta.2012.03.001

Lampert, M. A. (1956). Simplified Theory of Space-Charge-Limited Currents in an Insulator with Traps. *Physical Review Letters, 103*(6), 1648-1656. doi:https://doi.org/10.1103/PhysRev.103.1648

Lee, D., Park, J-W., Cho, N-K., Lee, J., Kim, Y.S. (2019). Verification of Charge Transfer in Metal-Insulator-Oxide Semiconductor Diodes via Defect Engineering of Insulator. *Scientific Reports, 9*, 1-9. doi:https://doi.org/10.1038/s41598-019-46752-1

Li, Y., Wang, Y., Fu, L., Chen, C., Yuan, P., Gao, X. . (2016). Research on Feasibility of Using a Transient Voltage Suppressor as the Selection Device for Bipolar RRAM. *Microelectronic Engineering, 164*, 20-22. doi:https://doi.org/10.1016/j.mee.2016.06.012

Liou, J. J. O.-C., A., Garcia-Sanchez F. (1998). MOSFET Physics and Modelling *Analysis and Design of MOSFETS*. Boston, MA: Springer.

Lu, A. H., Salabas, E.L., Schuth, F. (2007). Magnetic Nanoparticles: Synthesis, Protection, Functionalization, and Application. *Angewandte Chemie, 46*(8), 1222-1244. doi:https://doi.org/10.1002/anie.200602866

Ma, F. X., Hu, H., Wu, H.B., Xu, C.Y., Xu, Z., Zhen, L, David, L.X.W. (2015). Formation of Uniform Fe3O4 Hollow Spheres Organized by Ultrathin Nanosheets and Their Excellent Lithium Storage Properties. *Advanced Materials, 27*(27), 4097-4101. doi:https://doi.org/10.1002/adma.201501130

Manikanthababu, N., Tak, B.R., Prajna, K., Singh, R., Panigrahi, B.K. . (2020). Radiation Sustenance of HfO2/β-Ga2O3 Metal Oxide Semiconductor Capacitors: Gamma Irradiation Study. *Semiconductor Science and Technology, 35*(5), 1-22. doi:https://doi.org/10.1088/1361-6641/ab7b8b

Miozzo, L., Yassar, A., Horowitz, G. (2010). Surface Engineering for High Performance Organic Electronic Devices: The Chemical Approach. *Journal of Materials Chemistry, 20*(13), 2513-2538. doi:https://10.1039/b922385a

Murray A.F., R., H.M. (1987). Introduction to MOS (Metal-Oxide Semiconductor) Devices and Logic *Integrated Circuit Design*. New York, NY: Springer.

Neamen, D. A. (2012). Semiconductor Physics and Devices: Basic Principles. In M. Lange (Ed.), (Fourth Edition ed.). New York, NY: McGraw Hill.

Nemethova, V., Buliakova, B., Mazancova, P., Babelova, A., Selc, M., Moracikova, D., Klescikova, L., Ursinyova, M., Gabelova, A., Razga, F. . (2017). Intracellular Uptake of Magnetite Nanoparticles: A Focus on Physio-Chemical Characterization and Interpretation of In Vitro Data. *Materials Science and Engineering, 70*, 161-168. doi:https://doi.org/10.1016/j.msec.2016.08.064

Pakma, O. (2012). Current Mechanism in HfO2-Gated Metal-Oxide-Semiconductor Devices. *International Journal of Photoenergy, 2012*, 1-7. doi:https://doi.org/10.1155/2012/858350

Pang, Y. L., Lim, S., Ong H.C., Chong, W.T. . (2016). Research Progress on Iron Oxide-Based Magnetic Materials: Synthesis Techniques and Photocatalytic Applications. *Ceramics International, 42 A*(1), 9-34. doi:https://doi.org/10.1016/j.ceramint.2015.08.144

Pichon, B., Buchwalter, P., Carcel, C., Cattoen, X., Man, M.W.C., Begin-Colin, S. . (2012). Assembling of Magnetic Iron Oxide Nanoparticles Controlled by Self Assembled Monolayers of Functional Coordinating or Chelating Trialkoxysilanes. *The Open Surface Science Journal, 4*, 35-41. doi:10.2174/1876531901204010035

Ravindra, N. M. a. Z., J. (1992). Fowler-Nordheim Tunneling in Thin SiO2 Films. *Smart Materials and Structures, 1*(3), 197-201.

Reed, M. L., & Fedder, G. K. (1998). 2 - Photolithographic Microfabrication. In T. Fukuda & W. Menz (Eds.), *Handbook of Sensors and Actuators* (Vol. 6, pp. 13-61): Elsevier Science B.V.

Robertson, J. (2004). High Dielectric Constant Oxides. *The European Physical Journal Applied Physics, 28*, 265-291. doi:10.1051/epjap:2004206

Sah, C. T. (1964). Characteristics of the Metal-Oxide-Semiconductor Transistor. *IEEE Transactions on Electron Devices, 11*(7), 324-345. doi:10.1109/T-ED.1964.15336

Schroder, D. K. (2006). Semiconductor Material and Device and Characterization (Third Edition ed., pp. 790). Hoboken, New Jersey: John Wiley and Sons, Inc.

Simmons, J. G. (1965). Richardson-Schottky Effect in Solids. *Physical Review Letters, 15*(25), 967-968. doi:https://doi.org/10.1103/PhysRevLett.15.967

Sun, S. (2006). Recent Advances in Chemical Synthesis, Self-Assembly and Applications of FePt Nanoparticles. *Advanced Materials, 18*(4), 393-403. doi: https://doi.org/10.1002/adma.200501464

Terris, B. D., Thomson, T. (2005). Nanofabricated and Self-Assembled Magnetic Structures as Data Storage Media. *Journal of Physics D: Applied Physics, 38*(12), 199-222. doi:https://10.0.4.64/0022-3727/38/12/R01

Wong, Y. H., Cheong, K.Y. (2010). ZrO2 Thin Films on Si Substrate. *J Mater Sci: Mater Electron, 21*, 980-993. doi:10.1007/s10854-010-0144-5

Wong, Y. H., Cheong, K.Y. (2011). Electrical Characteristics of Oxidized/Nitrided Zr Thin Film on Si. *Journal of the Electrochemical Society, 158*, 1270-1278. doi:10.1149/2.106112jes

Xuan, M. (2020, 21 October 2020). Metal Oxide Semiconductor (MOS) Fundamentals. Retrieved from https://eng.libretexts.org/Bookshelves/Materials_Science/Supplemental_Modules_(Materials_Science)/Semiconductors/Metal-Oxide-Semiconductor_(MOS)_Fundamentals

Zafar, S., Jones, R.E., Jiang, B., White, B., Kaushik, V., Gillespie, S. (1998). The Electronic Conduction Mechanism in Barium Strontium Titanate Thin Films. *Applied Physics Letters, 73*(24), 3533-3535. doi:https://doi.org/10.1063/1.122827